

## Differing Reactions of Functionalized Hydrocarbons with $\text{Cp}^*\text{M}(\text{NO})(\text{alkyl})(\eta^3\text{-allyl})$ Complexes of Molybdenum and Tungsten

Tommy Tran,<sup>‡</sup> Catherine Chow,<sup>‡</sup> Amanda C. Zimmerman,<sup>‡</sup> Michelle E. Thibault,<sup>‡</sup>  
W. Stephen McNeil,<sup>\*,§</sup> and Peter Legzdins<sup>\*,‡</sup>

<sup>‡</sup>*Department of Chemistry, The University of British Columbia, Vancouver, British Columbia, Canada V6T 1Z1, and* <sup>§</sup>*Department of Chemistry, The University of British Columbia, Okanagan, Kelowna, British Columbia, Canada V1V 1V7*

Received September 21, 2010

$\text{Cp}^*\text{W}(\text{NO})(\text{CH}_2\text{CMe}_3)(\eta^3\text{-CH}_2\text{CHCHMe})$  (**1**) is known to initiate facile and selective aliphatic C–H bond activations of hydrocarbons at ambient temperatures. Its ability to effect C–H activations of unfunctionalized hydrocarbon portions of more complex molecules containing various functional groups has now been investigated in some detail. In addition, molybdenum analogues of **1** have also been examined in order to see how the C–H activation chemistry is affected when the central metal is changed. Thermolyses of **1** in neat 1-chloropropane, 1-chlorobutane, and 1-bromobutane at room temperature result in activation of the terminal C–H bonds at the end opposite the carbon–halogen linkage and the clean formation of the alkyl-allyl complexes  $\text{Cp}^*\text{W}(\text{NO})(\text{CH}_2\text{CH}_2\text{CH}_2\text{Cl})(\eta^3\text{-CH}_2\text{CHCHMe})$  (**2**),  $\text{Cp}^*\text{W}(\text{NO})(\text{CH}_2(\text{CH}_2)_2\text{CH}_2\text{Cl})(\eta^3\text{-CH}_2\text{CHCHMe})$  (**3**), and  $\text{Cp}^*\text{W}(\text{NO})(\text{CH}_2(\text{CH}_2)_2\text{CH}_2\text{Br})(\eta^3\text{-CH}_2\text{CHCHMe})$  (**4**), respectively. No reaction occurs with the C–Cl or C–Br bonds in the haloalkanes even though they are weaker than the C–H bonds that are activated. Similarly, treatment of **1** with *n*-Bu<sub>2</sub>O yields exclusively the terminal  $\text{sp}^3$  C–H activated product,  $\text{Cp}^*\text{W}(\text{NO})((\text{CH}_2)_4\text{O}(\text{CH}_2)_3\text{CH}_3)(\eta^3\text{-CH}_2\text{CHCHMe})$  (**5**), whereas the reaction with THF results in the single activation of a secondary  $\text{sp}^3$  C–H bond  $\alpha$  to the oxygen atom in THF and the formation of  $\text{Cp}^*\text{W}(\text{NO})(\text{C}_4\text{H}_7\text{O})(\eta^3\text{-CH}_2\text{CHCHMe})$  (**6**). Consistently, reaction of **1** with ethylcyclohexane results in preferential activation of one of the primary  $\text{sp}^3$  C–H linkages of the ethyl group and the formation of  $\text{Cp}^*\text{W}(\text{NO})(\text{CH}_2\text{CH}_2\text{C}_6\text{H}_{11})(\eta^3\text{-CH}_2\text{CHCHMe})$  (**7**). The  $\text{Cp}^*\text{Mo}(\text{NO})(\text{alkyl})(\eta^3\text{-allyl})$  complexes analogous to **1** are generally thermally unstable and react at or slightly above room temperature. The first member of this family of complexes to be studied was  $\text{Cp}^*\text{Mo}(\text{NO})(\text{CH}_2\text{CMe}_3)(\eta^3\text{-C}_3\text{H}_5)$  (**8**), whose thermolysis in the presence of pyridine at 35 °C over 3 days leads to the formation of  $\text{Cp}^*\text{Mo}(\text{NO})(\text{C}_5\text{H}_5\text{N})(\eta^2\text{-CH}_2=\text{CHCH}_2\text{CH}_2\text{-}t\text{-Bu})$  (**9**), an  $\eta^2$ -olefin complex in which the allyl and neopentyl ligands have coupled. The related  $\text{Cp}^*\text{Mo}(\text{NO})(\text{CH}_2\text{SiMe}_3)(\eta^3\text{-CH}_2\text{CHCHMe})$  complex (**11**) exists as a 2:1 mixture of isomers distinguishable by the orientation of the *endo*, *syn* allyl ligand. In the less sterically congested major isomer, the methyl group on the allyl ligand is adjacent to the NO ligand, but in the minor isomer the methyl group is adjacent to the more sterically demanding  $\text{CH}_2\text{SiMe}_3$  ligand. In general, the thermal reaction of **11** is similar to that of **1**. Spectroscopic monitoring indicates that the loss of TMS from **11** at room temperature results in the formation of a 16e  $\eta^2$ -diene intermediate complex that can be trapped with  $\text{PMe}_3$  as an 18e adduct,  $\text{Cp}^*\text{Mo}(\text{NO})(\eta^2\text{-CH}_2=\text{CHCH}=\text{CH}_2)(\text{PMe}_3)$  (**12**). However, reactions of **11** with various substrates (e.g., pentane, Et<sub>2</sub>O, and mesitylene) all lead to a single product,  $\text{Cp}^*\text{Mo}(\text{NO})(\eta^4\text{-trans-butadiene})$  (**13**). Evidently, the formation of the 18e butadiene complex is favored over the activation of a relatively electron-poor C–H bond by this molybdenum system. The results of DFT calculations on the model reaction of  $\text{CpW}(\text{NO})(\eta^2\text{-CH}_2=\text{CHCH}=\text{CH}_2)$  with propane confirm that the rate-determining step is the cleavage of a propane C–H bond and that the activation barrier for terminal activation is 8.6 kJ/mol lower in energy than that for internal activation. All new complexes have been characterized by conventional spectroscopic and analytical methods, and the solid-state molecular structures of complexes **3**, **5**, **6**, **8**, **9**, and **13** have been established by X-ray crystallographic analyses.

### Introduction

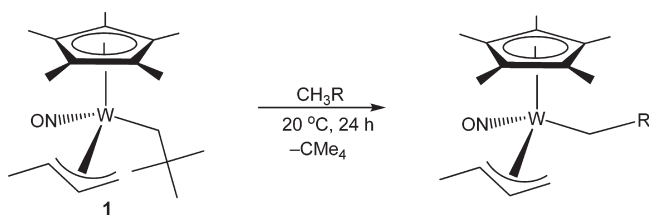
Current interest in effecting the activation and functionalization of hydrocarbon C–H bonds continues unabated

primarily because such capability holds the potential to considerably increase the number of synthetic pathways to

\*To whom correspondence should be addressed. E-mail: stephen.mcnail@ubc.ca; legzdins@chem.ubc.ca.

(1) See, for example: (a) Crabtree, R. H. *J. Chem. Soc., Dalton Trans.* **2001**, 17, 2437. (b) Labinger, J. A.; Bercaw, J. E. *Nature* **2002**, 417, 507. (c) Goldman, A.; Goldberg, K. I., Eds. *Activation and Functionalization of C–H Bonds*; American Chemical Society: Washington, DC, 2004. (d) Fekl, U.; Goldberg, K. I. *Adv. Inorg. Chem.* **2003**, 54, 259.

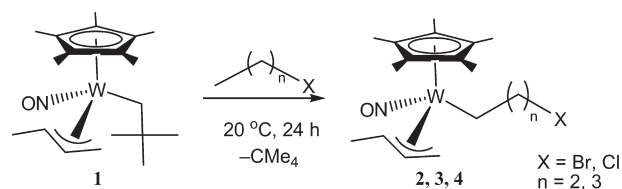
Scheme 1



a broad range of industrially important products beginning with relatively simple starting materials.<sup>1</sup> Saturated hydrocarbons, while abundant and relatively inexpensive, contain strong C–C and C–H bonds and lack Lewis-acidic or -basic reactive sites. They can be converted to other chemicals by employing highly reactive reagents or forcing experimental conditions, but these transformations generally lack selectivity and are often not compatible with other functional groups. Attention has therefore focused in recent years on utilizing transition-metal organometallic complexes for the activation and functionalization of inert C–H bonds of alkanes, and some notable successes have been achieved in this regard.<sup>2</sup> Thus, Shilov first demonstrated the possibility of catalytically converting methane to methyl chloride and methanol with an aqueous  $\text{Pt(II)/Pt(IV)}$  catalyst system.<sup>3</sup> In somewhat similar chemistry, Periana has shown that the oxidation of methane to methyl bisulfate can be effected in the presence of  $\text{Pt(II)}$  complexes bearing a bipyrimidine ligand.<sup>4</sup> Finally, Hartwig and co-workers have developed a series of group 6 and group 8 transition-metal complexes that mediate the conversion of alkanes to boronic esters either stoichiometrically or catalytically.<sup>5</sup>

Our recent contributions to this area of chemistry have involved the family of  $\text{Cp}^*\text{W}(\text{NO})(\text{alkyl})(\eta^3\text{-allyl})$  [ $\text{Cp}^* = \eta^5\text{-C}_5\text{Me}_5$ ] complexes,<sup>6</sup> which initiate various types of C–H activations. For instance, we have reported previously that the dimethylallyl complex  $\text{Cp}^*\text{W}(\text{NO})(\text{CH}_2\text{CMe}_3)(\eta^3\text{-CH}_2\text{-CHCMe}_2)$  generates two reactive intermediates upon thermolysis at  $50^\circ\text{C}$ , namely, a  $16e$   $\eta^2$ -allene complex and a  $16e$   $\eta^2$ -diene complex resulting from the loss of neopentane from the precursor compound. Under the experimental conditions employed, both intermediates show a marked preference for activating aryl C–H bonds and can also effect multiple C–H bond activations of saturated substrates.<sup>7</sup> In contrast, thermolysis of the monomethylallyl complex  $\text{Cp}^*\text{W}(\text{NO})(\text{CH}_2\text{CMe}_3)(\eta^3\text{-CH}_2\text{CHCHMe})$  (**1**) at ambient temperatures leads to the loss of neopentane and the formation of only the  $\eta^2$ -diene intermediate,  $\text{Cp}^*\text{W}(\text{NO})(\eta^2\text{-CH}_2=\text{CHCH}=\text{CH}_2)$ . In the presence of linear alkanes this intermediate complex effects C–H activations exclusively at the primary C–H bonds of the terminal carbons and forms

Scheme 2



$18e$   $\text{Cp}^*\text{W}(\text{NO})(n\text{-alkyl})(\eta^3\text{-CH}_2\text{CHCHMe})$  complexes (Scheme 1).<sup>8</sup> The newly formed alkyl ligands may be liberated from the tungsten centers in the product complexes as 1-iodoalkanes by treatment with elemental iodine.

We have subsequently extended our initial investigations with complex **1** in two different, but related, directions to delineate more fully the C–H activating capabilities of such monomethylallyl complexes. Specifically, we have first employed **1** itself to ascertain its ability to effect C–H activations of hydrocarbon portions of more complex molecules containing various functional groups. Second, we have also investigated molybdenum analogues of **1** to see how the C–H activation chemistry is affected when the metal is changed. In this report we present the results of these two investigations.

## Results and Discussion

**C–H Activation of Functionalized Hydrocarbons by  $\text{Cp}^*\text{W}(\text{NO})(\text{CH}_2\text{CMe}_3)(\eta^3\text{-CH}_2\text{CHCHMe})$  (**1**).** The monomethylallyl complex can be synthesized from  $\text{Cp}^*\text{W}(\text{NO})\text{Cl}_2$  via sequential metatheses with magnesium reagents, and it is isolable in moderate yields as an orange-yellow solid.<sup>8</sup> As a solid, it appears to be more thermally stable than originally reported, showing no noticeable signs of decomposition when stored under dinitrogen at ambient temperatures for two weeks. In solutions, however, it readily loses neopentane and forms the  $16e$  C–H activating complex  $\text{Cp}^*\text{W}(\text{NO})(\eta^2\text{-CH}_2=\text{CHCH}=\text{CH}_2)$ . In addition to assessing the behavior of this complex toward functionalized hydrocarbons, its selectivity toward different types of C–H linkages in these molecules also had to be ascertained.

**A. Activations of 1-Haloalkanes.** The activation of hydrocarbon C–H bonds in the presence of potentially reactive functional groups could provide new synthetic routes to more complicated organic compounds. Consequently, it is notable that thermolyses of **1** in neat 1-chloropropane, 1-chlorobutane, and 1-bromobutane at room temperature result in activation of the terminal C–H bonds at the end opposite the carbon–halogen linkage and the clean formation of the alkyl-allyl complexes  $\text{Cp}^*\text{W}(\text{NO})(\text{CH}_2\text{CH}_2\text{CH}_2\text{Cl})(\eta^3\text{-CH}_2\text{CHCHMe})$  (**2**),  $\text{Cp}^*\text{W}(\text{NO})(\text{CH}_2(\text{CH}_2)_2\text{CH}_2\text{Cl})(\eta^3\text{-CH}_2\text{CHCHMe})$  (**3**), and  $\text{Cp}^*\text{W}(\text{NO})(\text{CH}_2(\text{CH}_2)_2\text{CH}_2\text{Br})(\eta^3\text{-CH}_2\text{CHCHMe})$  (**4**), respectively (Scheme 2). An identical transformation occurs with 1-chloropentane.<sup>8</sup>

No reaction occurs with the C–Cl or C–Br bonds in the haloalkanes even though they are weaker than the C–H bonds that are activated.<sup>9</sup> In this regard the reactivity of complex **1** resembles that of the photochemically generated fragment  $[\text{Tp}'\text{Rh}(\text{CNR})]$  ( $\text{Tp}' = \text{hydrotris}(3,5\text{-dimethylpyrazolyl})\text{borate}$ ;  $\text{R} = \text{CH}_2\text{CMe}_3$ ) that Jones and co-workers have

(2) Hartwig, J. F. *Organotransition Metal Chemistry: From Bonding to Catalysis*; University Science Books: Sausalito, CA, 2010; Chapter 18.

(3) Shilov, A. E.; Shul'pin, G. B. *Chem. Rev.* **1997**, *97*, 2879, and references therein.

(4) Periana, R. A.; Taube, D. J.; Gamble, S.; Taube, H.; Satoh, T.; Fujii, H. *Science* **1998**, *280*, 560.

(5) (a) Sawyer, K. R.; Cahoon, J. F.; Shanoski, J. E.; Glascoe, E. A.; Kling, M. F.; Schlegel, J. P.; Zoerb, M. C.; Hapke, M.; Hartwig, J. F.; Webster, C. E.; Harris, C. B. *J. Am. Chem. Soc.* **2010**, *132*, 1848, and references therein. (b) Wei, C. S.; Jiménez-Hoyos, C. A.; Videa, M. F.; Hartwig, J. F.; Hall, M. B. *J. Am. Chem. Soc.* **2010**, *132*, 3078, and references therein.

(6) Tsang, J. Y. K.; Buschhaus, M. S. A.; Fujita-Takayama, C.; Patrick, B. O.; Legzdins, P. *Organometallics* **2008**, *27*, 1634.

(7) Ng, S. H. K.; Adams, C. S.; Hayton, T. W.; Legzdins, P.; Patrick, B. O. *J. Am. Chem. Soc.* **2003**, *125*, 15210.

(8) Tsang, J. Y. K.; Buschhaus, M. S. A.; Graham, P. M.; Semiao, C. J.; Semproni, S. P.; Kim, S. J.; Legzdins, P. *J. Am. Chem. Soc.* **2008**, *130*, 3652.

(9) *Mechanism and Theory in Organic Chemistry*, 3rd ed.; Lowry, T. H., Richardson, K. S., Eds.; Harper and Row: New York, 1987.

shown to react with 1-chloroalkanes to produce mostly terminal C–H activation products.<sup>10</sup> The solid-state molecular structure of complex **3** has been established by an X-ray crystallographic analysis and is shown in Figure 1.

As in other Cp\*W(NO)(alkyl)( $\eta^3$ -allyl) complexes,<sup>6</sup> the allyl ligand of complex **3** is in an *endo* orientation with the *meso* proton on C13 pointing away from the cyclopentadienyl ring (see Figure 1). Furthermore, there is a  $\sigma$ – $\pi$  distortion of the allyl ligand brought about by the electronic asymmetry at the metal center.<sup>11</sup> Because of this asymmetry, the bond distance C(14)–C(13) is 1.374 Å, whereas the bond length C(13)–C(12) is 1.416 Å. The spectroscopic properties of complexes **2**–**4** indicate that they are isostructural and that they retain their “piano-stool” molecular structures in solutions. In particular, their <sup>13</sup>C APT NMR spectra confirm that activation has occurred at the terminal C–H linkages.

**B. Activation of Di-*n*-butyl Ether.** The preference of complex **1** for activating primary sp<sup>3</sup> C–H bonds in linear alkanes also extends to di-*n*-butyl ether. Thus, just as for Et<sub>2</sub>O,<sup>8</sup> treatment of **1** with *n*-Bu<sub>2</sub>O yields exclusively the terminal sp<sup>3</sup> C–H activated product Cp\*W(NO)((CH<sub>2</sub>)<sub>4</sub>O(CH<sub>2</sub>)<sub>3</sub>CH<sub>3</sub>)( $\eta^3$ -CH<sub>2</sub>CHCHMe) (**5**) (Scheme 3). The <sup>13</sup>C APT NMR spectrum of **5** is also fully consistent with exclusive terminal C–H activation.

The ORTEP diagram of the solid-state molecular structure of **5** is shown in Figure 2. As for complex **3** (Figure 1),

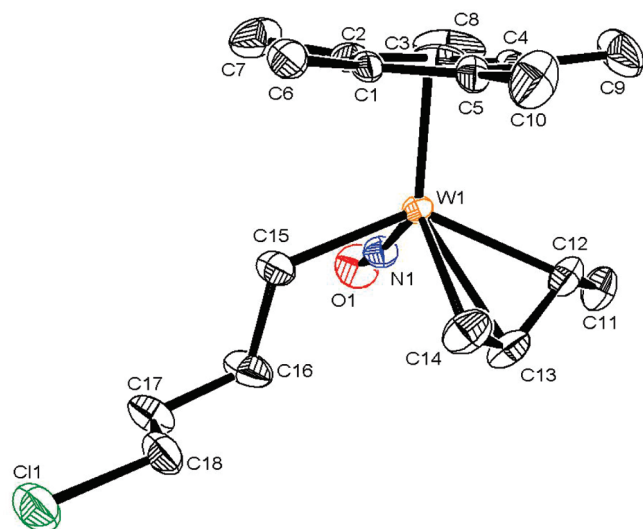


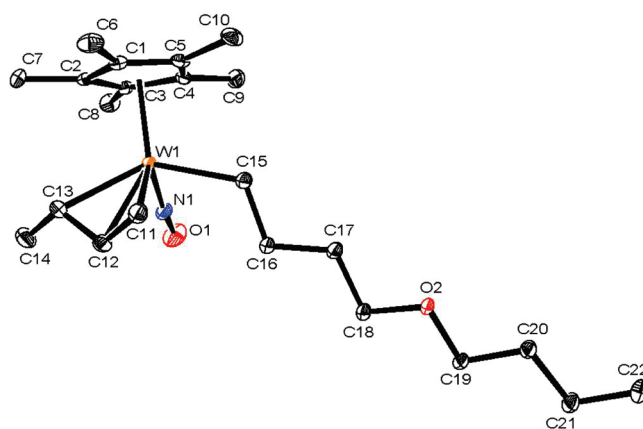
**Figure 1.** Solid-state molecular structure of complex **3** with 50% probability thermal ellipsoids. Selected interatomic distances (Å) and angles (deg): W(1)–C(14) = 2.331(3), W(1)–C(13) = 2.305(3), W(1)–C(12) = 2.276(3), W(1)–C(15) = 2.228(3), W(1)–N(1) = 1.777(2), N(1)–O(1) = 1.216(3), C(14)–C(13) = 1.381(5), C(13)–C(12) = 1.415(5), C(14)–C(13)–C(12) = 118.3(3), C(13)–C(12)–C(11) = 120.9(3), W(1)–N(1)–O(1) = 170.8(2).

the allyl ligand in **5** is bound in an *endo* conformation with the *meso* proton on the central carbon atom pointing away from the Cp\* ring, and it also displays the customary  $\sigma$ – $\pi$  distortion.

**C. Activation of THF and Ethylcyclohexane.** The reaction of **1** with THF (Scheme 4) illustrates that secondary C–H linkages can be activated when primary sp<sup>3</sup> C–H bonds are not present in the organic substrate. Hence, treatment of complex **1** with THF at room temperature affords **6** as a yellow powder whose <sup>13</sup>C APT NMR spectrum in C<sub>6</sub>D<sub>6</sub> indicates that the single activation of a C–H bond  $\alpha$  to the oxygen atom in THF has occurred. This reactivity contrasts with that described for the linear ether in the previous section in which only terminal C–H activation is observed. Complex **6** is formed as two diastereomers whose closest packing with their respective enantiomers constitutes the crystal structure of the compound. The solid-state molecular structure of one of these isomers is shown in Figure 3.

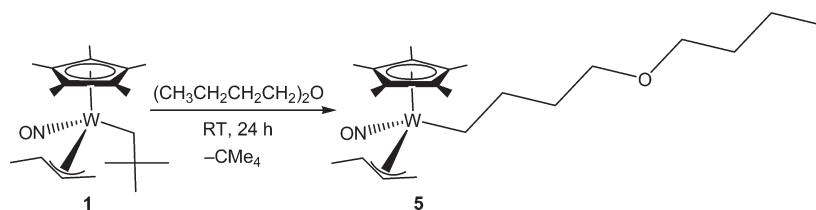
Interestingly, introduction of a saturated alkyl substituent onto a cyclohexane ring results in preferential activation of one of the primary sp<sup>3</sup> C–H linkages of the substituent (Scheme 5). Thus, treatment of **1** with ethylcyclohexane for a period of 24 h at ambient temperatures results in the isolation of complex **7** in 82% yield. The spectroscopic properties of **7** and its <sup>13</sup>C APT NMR spectrum (Figure 4) are fully consistent with only primary sp<sup>3</sup> C–H activation of the organic substrate having been effected.

**Analogous Cp\*Mo(NO)(alkyl)( $\eta^3$ -allyl) Complexes.** The C–H activating properties of the molybdenum analogues of tungsten complex **1** are of interest since we have previously



**Figure 2.** Solid-state molecular structure of **5** with 50% probability thermal ellipsoids. Selected interatomic distances (Å) and angles (deg): W(1)–C(11) = 2.363(2), W(1)–C(12) = 2.328(2), W(1)–C(13) = 2.284(2), W(1)–C(15) = 2.230(2), W(1)–N(1) = 1.7816(19), N(1)–O(1) = 1.217(2), C(11)–C(12) = 1.392(3), C(12)–C(13) = 1.420(3), C(13)–C(14) = 1.505(3), C(11)–C(12)–C(13) = 118.8(2), C(12)–C(13)–C(14) = 120.6(2), W(1)–C(15)–C(16) = 117.12(13), W(1)–N(1)–O(1) = 170.14(18).

**Scheme 3**





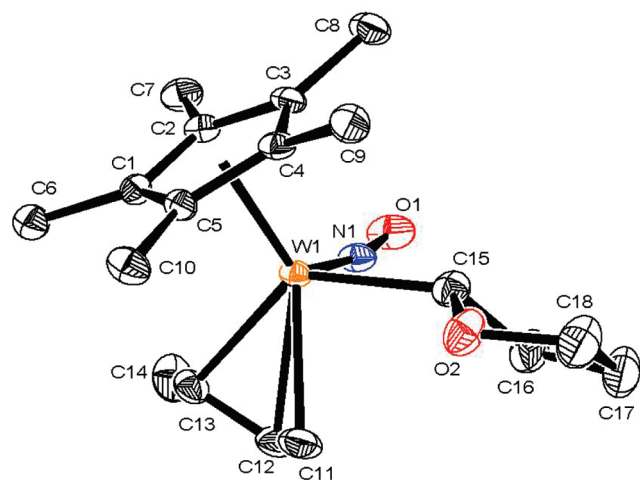
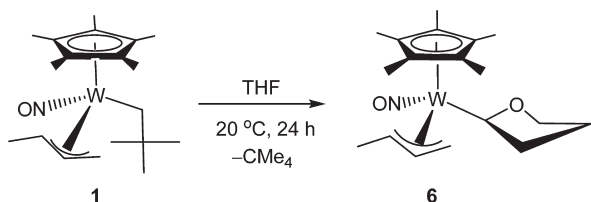


**Figure 3.** Solid-state molecular structure of **6** with 50% probability thermal ellipsoids. Selected interatomic distances (Å) and angles (deg): W(1)–C(11) = 2.353(6), W(1)–C(12) = 2.318(3), W(1)–C(13) = 2.279(3), W(1)–C(15) = 2.214(3), W(1)–N(1) = 1.774(2), N(1)–O(1) = 1.226(3), C(11)–C(12) = 1.383(5), C(12)–C(13) = 1.422(5), C(13)–C(14) = 1.509(4), C(15)–O(2) = 1.459(3), C(15)–C(16) = 1.532(4), C(11)–C(12)–C(13) = 118.2(3), C(12)–C(13)–C(14) = 120.0(3), W(1)–C(15)–C(16) = 118.9(2), W(1)–C(15)–O(2) = 117.76(19), W(1)–N(1)–O(1) = 169.4(2).

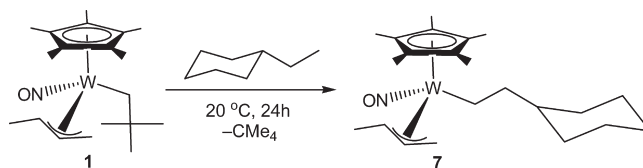
Scheme 4



demonstrated that molybdenum systems generally react similarly to their tungsten counterparts, but under gentler conditions.<sup>12</sup> This feature makes molybdenum compounds better candidates for eventual incorporation into catalytic systems since their higher activity could translate into larger turnover numbers or frequencies. Consequently, the initial goal of this part of the investigation was to identify a Cp\*Mo(NO)(alkyl)( $\eta^3$ -allyl) complex that performs selective C–H activations of hydrocarbons under ambient conditions.

The syntheses of the 18e Cp\*Mo(NO)(allyl)(alkyl) complexes can be achieved through sequential metatheses from Cp\*Mo(NO)Cl<sub>2</sub> with appropriate magnesium reagents (Scheme 6). The alkyl ligands used have been either the neopentyl group (CH<sub>2</sub>CMe<sub>3</sub>) or its silicon congener (CH<sub>2</sub>SiMe<sub>3</sub>). The intermediate 16e complexes, Cp\*Mo(NO)(alkyl)Cl, have not been isolated due to concerns about their thermal stability. It has previously been found that the formation of a molybdenum monoalkyl halo complex from the dihalide complex is temperature sensitive; above –50 °C the bis-alkyl

Scheme 5



product is formed.<sup>13</sup> Fortunately, isolation is not necessary in this instance if the species generated *in situ* is immediately reacted with the binary magnesium allyl reagent. Nevertheless, <sup>1</sup>H NMR spectroscopic analysis of the product mixtures often indicates the presence of the bis-alkyl products, even after chromatography of the final reaction mixtures on silica.

The allyl ligands were selected on the basis of reactivity displayed by the tungsten systems. Tungsten complexes containing allyl ligands with terminal methyl groups (*vide supra*) have been most thoroughly studied, so molybdenum analogues were synthesized to assess the metal's effect on the characteristic reactivity of the complex. The Cp\*Mo(NO)-(alkyl)( $\eta^3$ -allyl) complexes are generally thermally unstable and react at or slightly above room temperature. Hence, during the preparations of these compounds cold solvents must be utilized throughout.

**A. Cp\*Mo(NO)(CH<sub>2</sub>CMe<sub>3</sub>)( $\eta^3$ -C<sub>3</sub>H<sub>5</sub>) (8).** The first member of this family of complexes to be studied was complex **8**, which can be isolated as orange crystals. These crystals are relatively thermally stable in the solid state, but in solutions they begin to react at temperatures as low as 30 °C. The solid-state molecular structure of **8** is shown in Figure 5. The structure is similar to those exhibited by other complexes of this type (*vide supra*) in terms of the conformation and distortion of the allyl ligand, and the spectral features of **8** resemble those displayed by the previously reported tungsten congeners;<sup>6</sup> most distinctive is the presence of a multiplet at 4.99 ppm in the <sup>1</sup>H NMR spectrum of **8** in C<sub>6</sub>D<sub>6</sub> due to the *meso* proton on the allyl ligand.

Thermolysis of **8** in C<sub>6</sub>H<sub>6</sub> or C<sub>6</sub>D<sub>6</sub> in the presence of pyridine at 35 °C over 3 days leads to the formation of Cp\*Mo(NO)(C<sub>5</sub>H<sub>5</sub>N)( $\eta^2$ -CH<sub>2</sub>=CHCH<sub>2</sub>CH<sub>2</sub>-*t*-Bu) (**9**), an  $\eta^2$ -olefin complex in which the allyl and neopentyl ligands have coupled. This formulation is well-supported by the bond lengths in the solid-state molecular structure (Figure 6). Not only is the Mo center equidistant from the two carbon atoms C(11) and C(12), the interatomic distance between C(11) and C(12) is consistent with an elongated C=C double bond. The coupling of the two ligands likely occurs through pyridine-promoted nucleophilic attack of the neopentyl ligand on the allyl ligand, a process that may well be facilitated by the allyl ligand undergoing an  $\eta^3 \rightarrow \eta^1$  change in hapticity. Similar spectroscopic results are obtained during the thermolysis of **8** in C<sub>6</sub>D<sub>6</sub> in the presence of PMe<sub>3</sub>. At 35 °C over a period of 3 days, **8** is converted to a single organometallic product, which was initially formulated as the  $\eta^1$ -allyl PMe<sub>3</sub> adduct Cp\*Mo(NO)( $\eta^1$ -C<sub>3</sub>H<sub>5</sub>)(CH<sub>2</sub>CMe<sub>3</sub>)(PMe<sub>3</sub>). However, comparison of the product's spectroscopic properties with those of **9** and the PMe<sub>3</sub>  $\eta^2$ -diene complex **12** (*vide infra*) suggests that the analogous  $\eta^2$ -olefin complex, Cp\*Mo(NO)(PMe<sub>3</sub>)( $\eta^2$ -CH<sub>2</sub>=CHCH<sub>2</sub>CH<sub>2</sub>-*t*-Bu) (**10**), was also formed in this case.

(10) Vetter, A. J.; Rieth, R. D.; Brennessel, W. W.; Jones, W. D. *J. Am. Chem. Soc.* **2009**, *131*, 10742, and references therein.

(11) Semproni, S. P.; McNeil, W. S.; Baillie, R. A.; Patrick, B. O.; Campana, C. F.; Legzdins, P. *Organometallics* **2010**, *29*, 867.

(12) Legzdins, P.; Rettig, S. J.; Veltheer, J. E. *J. Am. Chem. Soc.* **1992**, *114*, 6922.

(13) Debad, J. D.; Legzdins, P.; Rettig, S. J.; Veltheer, J. E. *Organometallics* **1993**, *12*, 2714.

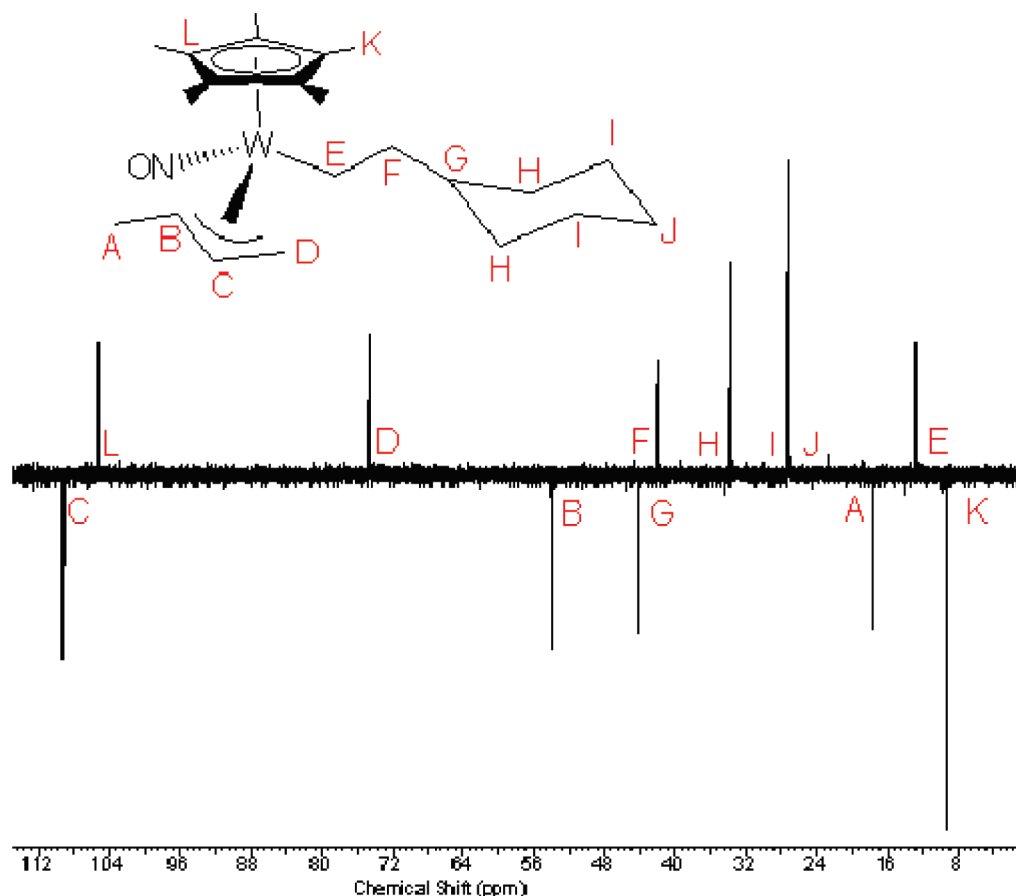
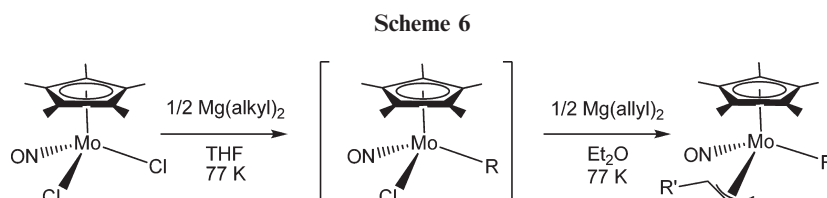


**Figure 4.**  $^{13}\text{C}$  APT NMR spectrum of complex **7** in  $\text{C}_6\text{D}_6$ . The resonances due to the carbons labeled as I and J are very close together.



Notably, there is no evidence for the activation of  $\text{C}_6\text{D}_6$  during either thermolysis; the only triplet (from C–D coupling) in the  $^{13}\text{C}\{^1\text{H}\}$  NMR spectrum is from the NMR solvent itself. In other words, none of the hydrogen atoms of the  $\eta^3\text{-C}_3\text{H}_5$  ligand in **8** are apparently situated in such a configuration that they can participate in metal-assisted elimination of neopentane from the molybdenum's coordination sphere in order to generate an intermediate allene complex capable of activating C–H bonds. Finally, it may be noted that complex **8** displays a much lower threshold for thermal reactivity than does its W congener; the latter is apparently stable for up to 16 h at 70 °C in both  $\text{C}_6\text{D}_6$  and neat  $\text{PMe}_3$ .<sup>6</sup>

**B.**  $\text{Cp}^*\text{Mo}(\text{NO})(\text{CH}_2\text{SiMe}_3)(\eta^3\text{-CH}_2\text{CHCHMe})$  (**11**). The thermal and C–H activating properties of **11** have been studied because of its similarity to tungsten complex **1** (*vide supra*). The exact molybdenum congener,  $\text{Cp}^*\text{Mo}(\text{NO})(\text{CH}_2\text{CMe}_3)(\eta^3\text{-CH}_2\text{CHCHMe})$ , has not been synthesized due to concerns about its thermal stability. It was hoped that

the replacement of the neopentyl ligand by the trimethylsilylmethyl group would decrease the reactivity of the complex sufficiently to lead to its isolation.<sup>14</sup>

Syntheses of **11** do not proceed cleanly, and the final product mixture typically contains some  $\text{Cp}^*\text{Mo}(\text{NO})(\text{CH}_2\text{SiMe}_3)_2$  even after having been chromatographed on silica. The presence of this byproduct is evident in the  $^1\text{H}$  NMR spectrum of the product mixture, which displays a characteristic doublet at  $-1.17$  ppm attributable to one of the diastereotopic protons of the  $\text{CH}_2\text{SiMe}_3$  ligand.<sup>15</sup>

Like some of the other complexes containing the  $\eta^3\text{-CH}_2\text{CHCHMe}$  ligand,<sup>6</sup> complex **11** exists as a 2:1 mixture of isomers distinguishable by the orientation of the *endo*, *syn* allyl ligand. In the major isomer, the methyl group on the allyl ligand is adjacent to the NO ligand, but in the minor isomer, the methyl group is adjacent to the more sterically demanding  $\text{CH}_2\text{SiMe}_3$  ligand.<sup>8</sup> The most evident manifestation of the mixture of isomers is the presence of a second set of signals in the  $^1\text{H}$  NMR spectrum attributable to the

(14) Wada, K.; Pamplin, C. B.; Legzdins, P.; Patrick, B. O.; Tsyba, I.; Bau, R. *J. Am. Chem. Soc.* **2003**, *125*, 7035.

(15) Legzdins, P.; Lundmark, P. J.; Phillips, E. C.; Rettig, S. J.; Veltheer, J. E. *Organometallics* **1992**, *11*, 2991.

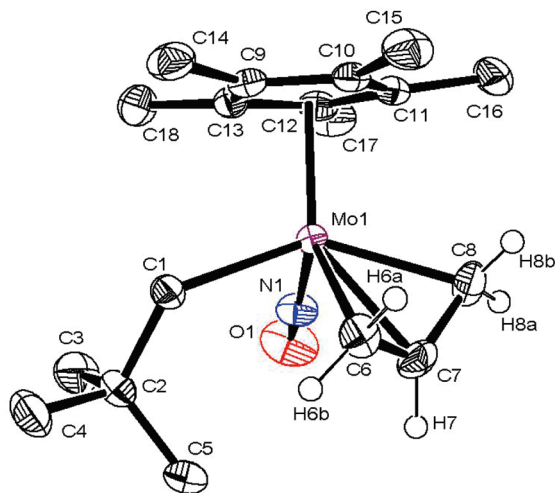


**Figure 5.** Solid-state molecular structure of **8** with 50% probability thermal ellipsoids. Selected interatomic distances (Å) and angles (deg): Mo(1)–C(6) = 2.407(3); Mo(1)–C(7) = 2.332(2); Mo(1)–C(8) = 2.261(3); C(6)–C(7) = 1.370(4); C(7)–C(8) = 1.405(4); N(1)–O(1) = 1.208(3); Mo(1)–N(1)–O(1) = 170.1(2); C(6)–C(7)–C(8) = 118.2(3).

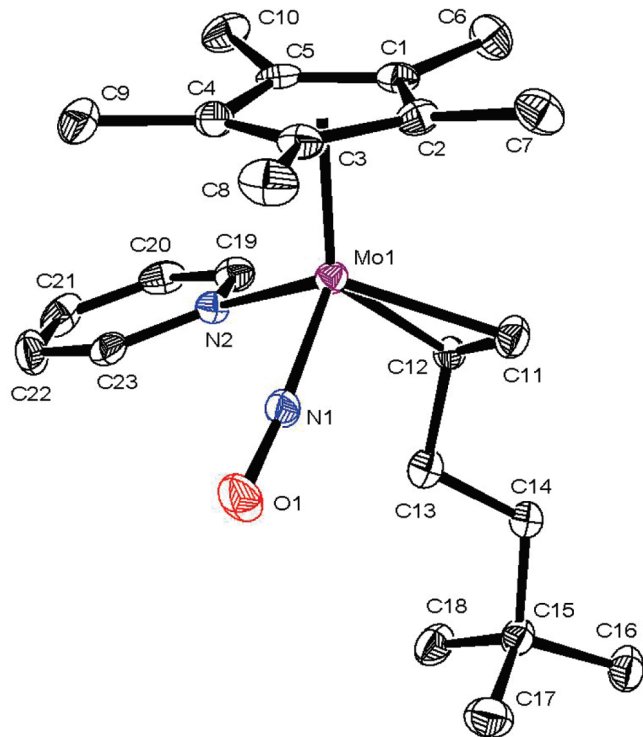


**Figure 6.** Solid-state molecular structure of **9** with 50% probability thermal ellipsoids. Selected interatomic distances (Å) and angles (deg): Mo(1)–C(11) = 2.203(3); Mo(1)–C(12) = 2.220(3); C(11)–C(12) = 1.422(5); C(12)–C(13) = 1.514(5); C(13)–C(14) = 1.531(5); N(1)–O(1) = 1.222(3); Mo(1)–N(2) = 2.200(3); Mo(1)–N(1) = 1.768(3); Mo(1)–N(1)–O(1) = 175.2(3); C(11)–C(12)–C(13) = 119.8(3).

diastereotopic protons on the  $\text{CH}_2\text{SiMe}_3$  ligand at  $-0.71$  and  $-0.40$  ppm; integration of one of these doublets against a doublet of the major product yields a 1:2 ratio.

Complex **11** is thermally unstable at room temperature and readily evolves TMS, a convenient feature when monitoring its reactions by  $^1\text{H}$  NMR spectroscopy. However, it

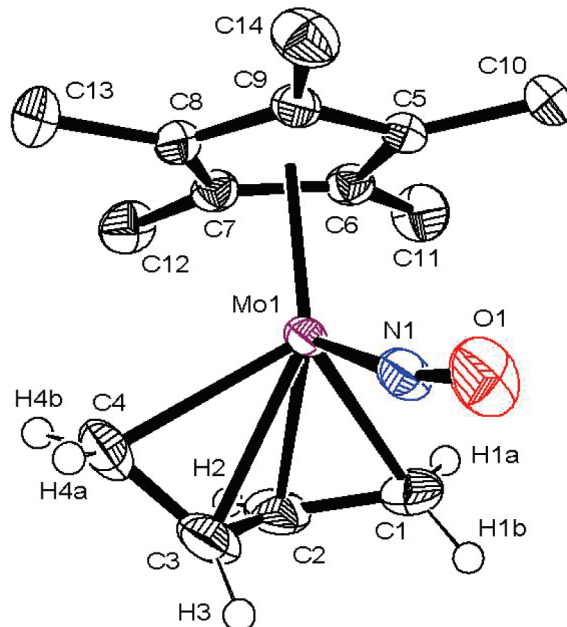
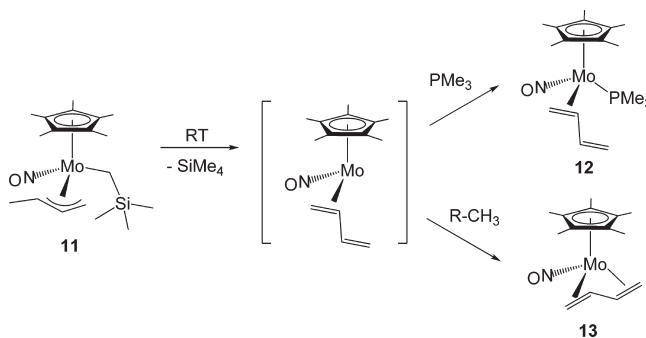


**Figure 7.** Solid-state molecular structure of **13** with 50% probability thermal ellipsoids. Selected interatomic distances (Å) and bond angles (deg): Mo(1)–C(1) = 2.3160(18); Mo(1)–C(2) = 2.1974(18); Mo(1)–C(3) = 2.2313(19); Mo(1)–C(4) = 2.2978(17); C(1)–C(2) = 1.404(3); C(3)–C(2) = 1.412(3); C(4)–C(3) = 1.398(3); Mo(1)–N(1)–O(1) = 168.36(13); C(1)–C(2)–C(3) = 121.31(18); C(2)–C(3)–C(4) = 118.98(18).

#### Scheme 7



can be stored for weeks in a pentane solution at  $-30\text{ }^\circ\text{C}$  without any significant degradation. In general, the thermal behavior of **11** is similar to that of **1**, spectroscopic monitoring indicating that the loss of TMS results in the formation of a  $16e$   $\eta^2$ -diene intermediate complex that can be trapped as an  $18e$  adduct (**12**) with  $\text{PMe}_3$  (Scheme 7). Not surprisingly, the  $^1\text{H}$  NMR spectrum of **12** in  $\text{C}_6\text{D}_6$  resembles that displayed by its W congener.<sup>8</sup> Specifically, three diagnostic downfield resonances between 4.5 and 6.1 ppm for the protons on the uncoordinated  $\text{H}_2\text{C}=\text{CH}$  unit of the diene ligand provide clear evidence for the formation of this compound.

On the basis of the thermal properties of **11**, it was hoped that the complex would perform C–H activations of alkanes in a manner similar to those effected by **1**. However, reactions of **11** with various substrates (e.g., pentane,  $\text{Et}_2\text{O}$ , and mesitylene) all lead to a single product,  $\text{Cp}^*\text{Mo}(\text{NO})(\eta^4\text{-trans-butadiene})$  (**13**) (Scheme 7, Figure 7). Evidently, the formation of the butadiene complex is favored over the

activation of a solvent C–H bond in this system. The formation of this product indicates that in the case of the molybdenum system the electron-deficient  $\eta^2$ -diene complex can more easily attain an 18e configuration by coordinating the other double bond of the diene ligand rather than by activating a relatively electron-poor C–H bond.

$\eta^4$ -*trans*-Diene complexes such as complex **13** have previously been prepared by reduction of  $\text{Cp}^*\text{Mo}(\text{NO})\text{I}_2$  with Na/Hg amalgam in the presence of excess dienes<sup>16</sup> and later through the treatment of  $\text{Cp}^*\text{M}(\text{NO})(\text{CH}_2\text{SiMe}_3)_2$  (M = Mo, W) with  $\text{H}_2$  in the presence of excess diene.<sup>17</sup> The  $\eta^4$ -*trans*-diene bonding motif is unusual in a transition-metal complex; *cis*-diene ligands are much more common.<sup>16</sup> In general, the group 6  $\eta^4$ -*trans*-butadiene complexes are kinetically inert with respect to ligand substitution.<sup>16</sup>

To ascertain whether any C–H activation can be effected with this system, the thermolysis of complex **11** in neat  $\text{C}_5\text{D}_{12}$  has been investigated. Reactant **11** is consumed via a pseudo-first-order process (Figure 8) with an observed rate constant of  $7.1(5) \times 10^{-5} \text{ s}^{-1}$  ( $R^2 = 0.987$ ). However, all the signals in the  $^{13}\text{C}\{^1\text{H}\}$  NMR spectrum of the final reaction mixture are singlets, thereby indicating that no deuterium incorporation and no C–D activation has occurred.

**Theoretical Investigations.** In an effort to better understand the observed selectivity of these C–H activation processes, a model reaction has been examined by DFT calculations in which the  $\text{Cp}^*$  is modeled by Cp and the alkyl fragment is provided by propane, which can activate at either a primary C–H bond to yield an *n*-propyl allyl complex or at a secondary C–H bond to afford an isopropyl allyl complex. A similar reaction profile has been previously investigated theoretically by Fan and Hall,<sup>18</sup> namely, the initial decomposition pathway of  $\text{CpW}(\text{NO})(\text{CH}_3)(\eta^3\text{-CH}_2\text{CHCMe}_2)$  to afford  $\text{CpW}(\text{NO})(\eta^2\text{-butadiene})$  and  $\text{CH}_4$ . These results showed a preferred pathway involving a tungsten-assisted transfer of one hydrogen atom from the allyl methyl group to the alkyl ligand, via an intermediate stabilized by a  $\beta$ -H agostic interaction. Our results mirror this preferred pathway, yielding the transformations shown

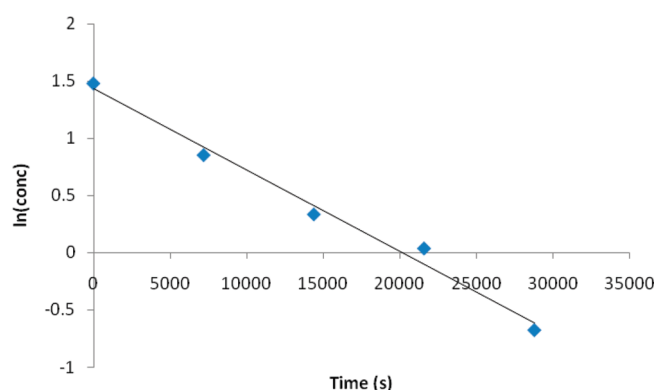


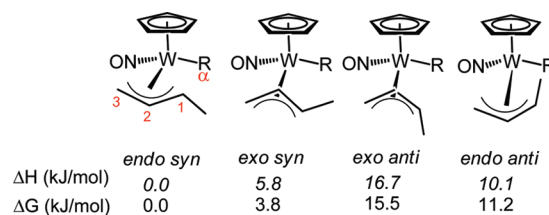
**Figure 8.** First-order rate law plot for the consumption of complex **11** during the reaction with  $\text{C}_5\text{D}_{12}$ .

in Scheme 8 for the conversion of  $\text{CpW}(\text{NO})(\text{C}_3\text{H}_7)(\eta^3\text{-CH}_2\text{CHCHMe})$  (**A**) to  $\text{CpW}(\text{NO})(\text{C}_3\text{H}_8)(\eta^2\text{-CH}_2\text{CHCH}_2)$  (**C**).

These transformations are potentially complicated by the availability of multiple allyl conformations in the initial alkyl allyl compound **A**, with the allyl group either *endo* or *exo*, the  $\text{CH}_3$  substituent on the allyl either *anti* or *syn* with respect to the *meso* proton, and the  $\text{CH}_3$  group either proximal to or distal from the alkyl ligand. Although most solid-state structures of various  $\text{Cp}^*\text{W}(\text{NO})(\text{methylallyl})(\text{R})$  complexes exhibit a distal methyl group, with the nitrosyl ligand between the allyl  $\text{CH}_3$  and the alkyl ligand (e.g., **3**, **5**, **6**, and structures in ref 6), the H-atom transfer between the allyl and the alkyl groups is obviously not possible unless the allyl begins with the methyl group in a proximal position. It is not immediately obvious for which of the remaining conformers the required H-atom transfer reaction would be viable or preferred. However, such conformations of  $\eta^3$ -allyl moieties in cyclopentadienyl metal complexes have been shown theoretically to have low interconversion barriers.<sup>19</sup> Thus, **11** exhibits both isomers in the solid state (*vide supra*). Also, when single crystals of the distal isomer of *endo syn*  $\text{Cp}^*\text{W}(\text{NO})(\text{C}_6\text{H}_5)(\eta^3\text{-CH}_2\text{CHCHMe})$  are dissolved in  $\text{C}_6\text{D}_6$  at room temperature,  $^1\text{H}$  NMR spectroscopy confirms that an equilibrium mixture of both proximal and distal isomers is established almost immediately.<sup>20</sup> In other words, it appears that the distal conformers, even if slightly more stable, can rapidly rearrange to the reactive proximal arrangement.

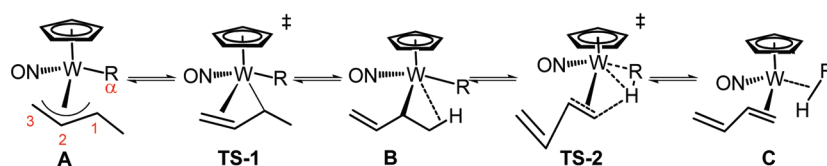
Optimizations of the model complex  $\text{CpW}(\text{NO})(n\text{-propyl})(\eta^3\text{-CH}_2\text{CHCHMe})$  (*n*-PrA) with all four proximal allyl conformations result in a slight preference for the *endo syn* arrangement (Figure 9), with the *exo syn* conformer about 4 kJ/mol higher in energy and the two *anti* conformers at 11 and 16 kJ/mol higher. The *exo anti* conformer, in addition to being the least stable, has the allyl methyl group oriented away from the propyl ligand, making a hydrogen-atom transfer reaction from this species unlikely.

This result is in slight contrast to the findings of Hall, who determined the *exo* arrangement to be slightly favored in  $\text{CpW}(\text{NO})(\text{CH}_3)(\eta^3\text{-CH}_2\text{CHCMe}_2)$  and an H-atom transfer from the *exo syn* methyl to be the most favorable pathway.<sup>18</sup> However, it should be noted that Hall's total calculated energy difference between the highest energy transition states



**Figure 9.** Calculated relative enthalpies and free energies (in kJ/mol) for model complex *n*-PrA with four different allyl conformations.

**Scheme 8**

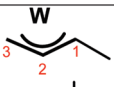
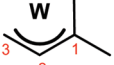




for the two *syn* H-atom transfer paths is only 3.3 kJ/mol. As well, the Hall model possesses an extra CH<sub>3</sub> group oriented directly toward the Cp ligand in an *endo* conformation, which could presumably serve as a slight destabilizing force. A direct comparison of the optimized structures for *endo syn* *n*-PrA and *endo* CpW(NO)(*n*-propyl)( $\eta^3$ -CH<sub>2</sub>CHCMe<sub>2</sub>), using the same method and basis set for both, reveals just such a destabilization. Relevant metrical parameters for the allyl group are shown in Table 1. The presence of the extra methyl group forces the position of the allyl group to shift such that it adopts a structure exhibiting slightly greater  $\sigma$ - $\pi$  distortion and a dramatically lengthened distance to the dimethyl carbon atom. Accordingly, we conclude that the loss of this methyl substituent in our model renders the *endo syn* arrangement more stable than the corresponding *exo* conformer, and we have therefore considered only the reaction coordinate for the *endo syn* pathway in all further calculations.

The loss of alkane from propyl allyl compounds **A** proceeds via a transition state **TS-1** in which two carbon atoms

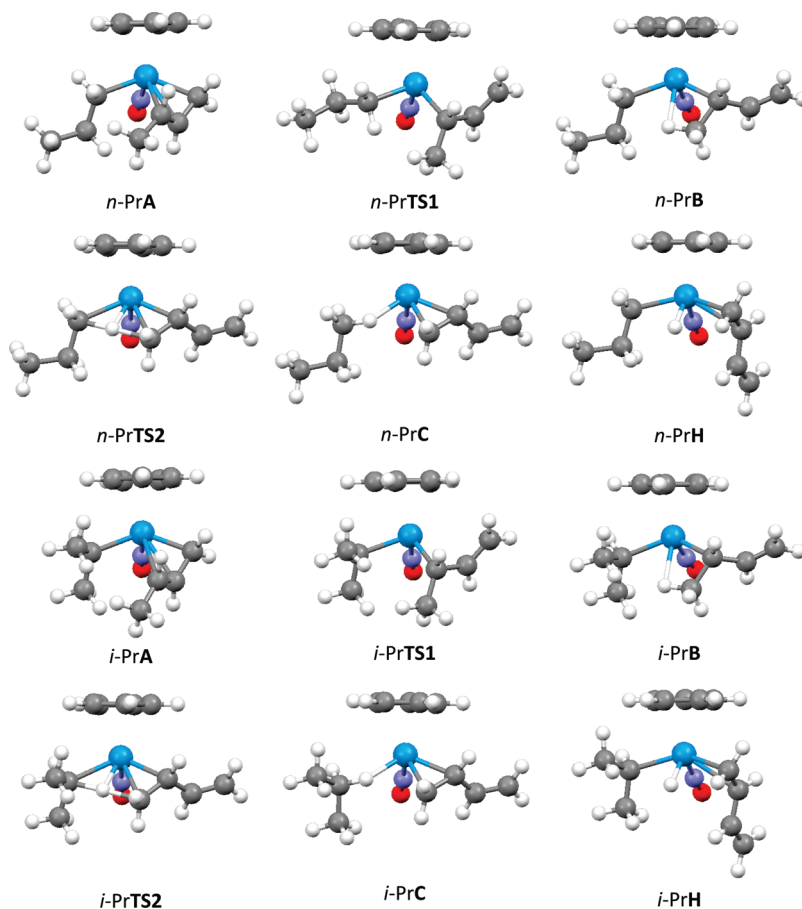
**Table 1.** Calculated Bond Lengths (pm) and Angles (deg) for the Allyl Group in *n*-PrA and CpW(NO)(*n*-propyl)( $\eta^3$ -CH<sub>2</sub>CHCMe<sub>2</sub>)

	W-C1	W-C2	W-C3	C1-C2	C2-C3	W-C3-C2
	268.7	243.5	222.2	138.9	146.4	79.8
	310.0	252.3	218.5	138.1	148.2	84.6

of the allyl moiety swing away from the metal and the pendant methyl group swings inward, leading to an  $\eta^1$ -alkyl with a  $\beta$ -agostic H on the methyl group (**B**) (Scheme 8). A second transition state (**TS-2**) has the  $\beta$ -agostic H move across the face of the tungsten atom toward the W-bound propyl carbon, leading to a propane sigma complex and an  $\eta^2$  diene ligand (**C**). Calculated structures for these complexes, for both the *n*-propyl and isopropyl cases, are shown in Figure 10. The calculated relative enthalpies and energies of these species, taking the energy of *n*-PrC as 0.0 kJ/mol, are indicated in Table 2 and are shown in Figure 11.

A discrete hydride compound **H** was also calculated to be a stable minimum-energy structure for both propyl isomers (Figure 10 and Table 2). However, these compounds have much higher energies than even the highest energy **TS-2** on both pathways, and there are no transition states connecting hydrides **H** to other species on the reaction coordinate (i.e., **B** and **C**). We therefore cannot consider these hydride complexes to play a role in the observed chemistry.

The reverse of the reaction shown in Scheme 8 is therefore the expected pathway by which the tungsten diene complex would activate the C-H bond of a new hydrocarbon fragment to yield alkyl allyl complexes such as **2-7**. The initial propane adducts have very nearly the same energy (less than 2 kJ/mol free energy difference), but along the C-H activation reaction coordinate there is a clear preference for the reaction of a primary C-H bond to form the *n*-propyl isomer rather than that of a secondary C-H bond to form the isopropyl compound. The preference is manifested both thermodynamically—the alkyl allyl product **C** favors the

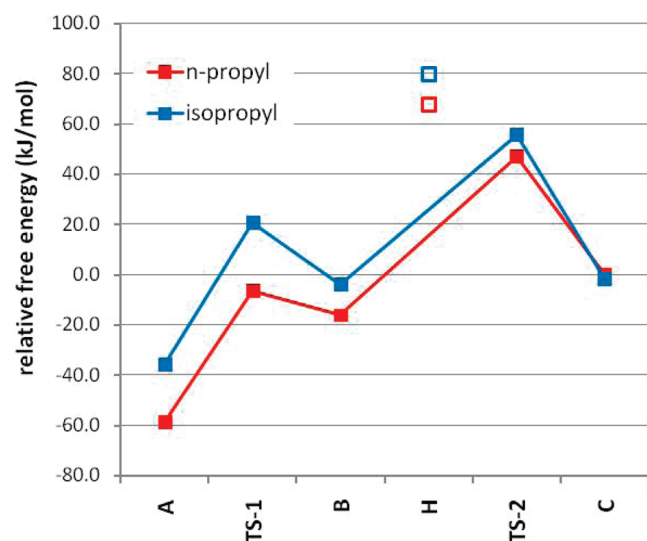


**Figure 10.** Structures of the complexes in Scheme 8 and the alkyl hydride complexes **H**.



**Table 2.** Relative Enthalpies and Energies (in kJ/mol) and Selected W–C Bond Lengths (in pm) of the Species Shown in Scheme 8 and the Alkyl Hydride Complexes H

	compound	$\Delta H$	$\Delta G$	W–C $\alpha$	W–C1
	<i>n</i> -PrA	–71.1	–58.7	222.6	269.7
	<i>i</i> -PrA	–43.9	–35.9	223.6	299.2
	<i>n</i> -PrTS-1	–18.6	–6.5	216.9	217.1
	<i>i</i> -PrTS-1	+5.1	+20.7	221.7	218.2
	<i>n</i> -PrB	–22.1	–16.1	220.3	216.7
	<i>i</i> -PrB	–12.1	–4.1	221.1	216.5
	<i>n</i> -PrTS-2	+37.6	+47.0	238.1	220.7
	<i>i</i> -PrTS-2	+42.8	+55.6	240.8	220.4
	<i>n</i> -PrC	0.0	0.0	288.0	221.8
	<i>i</i> -PrC	–3.3	–1.9	295.7	221.7
	<i>n</i> -PrH	+53.5	+67.7	222.7	257.8
	<i>i</i> -PrH	+69.0	+79.8	226.1	259.6

**Figure 11.** Reaction profile for the mechanism shown in Scheme 8. The comparative energies of the hydride complexes H are shown as open boxes.

*n*-propyl product by 22.8 kJ/mol—and kinetically—the initial TS1 favors primary activation by 8.6 kJ/mol. Assuming kinetic control of these reactions, such a barrier would predict a 97:3 ratio in favor of the *n*-propyl product, consistent with the essentially quantitative selectivity for pri-

mary C–H bonds that is experimentally observed during the formation of complexes **2**, **3**, **4**, **5**, and **7**.

We attribute these energy differences primarily to the additional steric strain required by the activation of a secondary C–H bond. On the isopropyl pathway, the alkyl fragment is generally positioned such that one methyl group is oriented down and away from the rest of the complex, which is the same position as the  $-\text{CH}_2\text{CH}_3$  group on the *n*-propyl pathway. The second methyl group in the isopropyl path is directed away from the nitrosyl ligand, with a C–C bond roughly parallel to the ring of the cyclopentadienyl group. Close examination of the W–C bond lengths shows a consistently greater distance to either the propyl  $\alpha$ -carbon or both the C $\alpha$  and the C1 of the allyl group along the isopropyl pathway (Table 2), consistent with a steric destabilization of a reaction pathway that passes a hydrogen atom between these two carbons. The steric effects of the proximity of this second methyl group to the Cp ring in these model complexes would presumably be exacerbated in the experimental Cp\* derivatives, further promoting the selectivity for primary C–H bonds.

It is also possible that the observed selectivity can be attributed in part to a complementary electronic effect, that of the differences in C–H and W–C bond enthalpies for the two modes of reactivity. The terminal C–H bond in propane is approximately 12 kJ/mol stronger than the internal C–H bond (422 vs 410 kJ/mol).<sup>21</sup> The corresponding W–C bonds would be expected to exhibit a similar enthalpic trend, with the product *i*-PrB having a stronger W–C bond than *n*-PrB. Given that the initial C–H activation transition state TS-1 involves partial formation of this W–C bond, the enthalpic preference for *i*-PrB would help to stabilize the corresponding transition state *i*-PrTS-1. Such a kinetic selectivity trend requires that product M–C bond enthalpies increase more rapidly than reactant H–C bond enthalpies, a conclusion borne out by numerous theoretical calculations on various C–H activation reactions.<sup>22</sup> However, such calculations have shown that the correlation line of calculated H–C and M–C bond enthalpies for simple hydrocarbons generally have slopes between 1.0 and 1.9, with slopes around 1.2 being most common. In other words, M–C bond enthalpies typically increase approximately 20% faster than H–C bond enthalpies. Given only a 12 kJ/mol difference in the initial C–H bonds to be broken, this could account for a 14 kJ/mol difference in M–C bonds to be formed and contribute a net 2 kJ/mol to the favored enthalpy of the *i*-PrB product. Our calculated energy difference favors *i*-PrB by 10.0 kJ/mol (Table 2), so we conclude that a substantial steric effect must also be required to explain the observed selectivity.

## Epilogue

In summary, we have demonstrated that at room temperature Cp\*W(NO)(CH<sub>2</sub>CMe<sub>3</sub>)( $\eta^3$ -CH<sub>2</sub>CHCHMe) (**1**) has a proclivity for initiating the clean C–H activations of the primary sp<sup>3</sup> C–H bonds of 1-bromobutane, 1-chlorobutane, 1-chloropropane, di-*n*-butyl ether, and ethylcyclohexane. When such C–H bonds are not present in the organic substrate, secondary sp<sup>3</sup> C–H linkages can be activated by **1**, the reaction with THF resulting in the single activation of a C–H bond  $\alpha$  to the oxygen atom. The results of DFT

(16) Christensen, N. J.; Hunter, A. D.; Legzdins, P. *Organometallics* **1989**, *8*, 930.

(17) Debad, J. D.; Legzdins, P.; Young, M. A.; Batchelor, R. J.; Einstein, F. W. B. *J. Am. Chem. Soc.* **1993**, *115*, 2051.

(18) Fan, Y.; Hall, M. B. *Organometallics* **2005**, *24*, 3827.

(19) Ariafard, A.; Bi, S.; Lin, Z. *Organometallics* **2005**, *24*, 2241.

(20) Baillie, R. A.; Tran, T.; Thibault, M. E.; Legzdins, P., unpublished observations.

(21) *CRC Handbook of Chemistry and Physics*, 91st ed., Internet Version 2011; Lide, D. R., Ed.; CRC Press: Boca Raton, FL, 2011; pp 9–71.

(22) Balcells, D.; Clot, E.; Eisenstein, O. *Chem. Rev.* **2010**, *110*, 749.

calculations on the model reaction of  $\text{Cp}^*\text{W}(\text{NO})(\eta^2\text{-CH}_2=\text{CHCH}=\text{CH}_2)$  with propane confirm that the rate-determining step is the cleavage of the first propane C–H bond and that the activation barrier for terminal activation is 8.6 kJ/mol lower in energy than that for internal activation. Disappointingly, analogous  $\text{Cp}^*\text{Mo}(\text{NO})(\text{alkyl})(\eta^3\text{-allyl})$  complexes do not initiate similar C–H activations. Thus, thermolysis of  $\text{Cp}^*\text{Mo}(\text{NO})(\text{CH}_2\text{CMe}_3)(\eta^3\text{-C}_3\text{H}_5)$  in  $\text{C}_6\text{D}_6$  in the presence of Lewis bases leads to their conversion to the  $\eta^2$ -olefin adducts  $\text{Cp}^*\text{Mo}(\text{NO})(\eta^2\text{-CH}_2=\text{CHCH}_2\text{CH}_2\text{-}t\text{-Bu})(\text{L})$ , there being no evidence for the activation of  $\text{C}_6\text{D}_6$ . More encouraging is the fact that the thermal behavior of  $\text{Cp}^*\text{Mo}(\text{NO})(\text{CH}_2\text{SiMe}_3)(\eta^3\text{-CH}_2\text{CHCHMe})$  (**11**) is similar to **1** in that it loses TMS at room temperature and forms a 16e  $\eta^2$ -diene intermediate complex that can be trapped as an 18e adduct by  $\text{PMe}_3$ . However, unlike for **1**, this  $\eta^2$ -diene compound rapidly converts to the 18e  $\text{Cp}^*\text{Mo}(\text{NO})(\eta^4\text{-trans-butadiene})$  complex rather than effecting the activation of the primary  $\text{sp}^3$  C–H bonds of a variety of substrates. The next step in these investigations is to determine the experimental conditions for releasing the alkyl ligands formed by the C–H activation processes from the tungsten's coordination spheres in an appropriately functionalized manner. Such studies are currently ongoing.

## Experimental Section

**General Methods.** All reactions and subsequent manipulations involving organometallic reagents were performed under anaerobic and anhydrous conditions under either high vacuum or an inert atmosphere of prepurified dinitrogen. Purification of inert gases was achieved by passing them first through a column containing MnO and then a column of activated 4 Å molecular sieves. Conventional glovebox and vacuum-line Schlenk techniques were utilized throughout. The gloveboxes used were Innovative Technologies LabMaster 100 and MS-130 BG dual-station models equipped with freezers maintained at  $-30^\circ\text{C}$ . Most of the reactions were performed in thick-walled glass vessels possessing Kontes greaseless stopcocks and side arm inlets for vacuum-line attachment. Small-scale reactions and NMR spectroscopic analyses were conducted in J. Young NMR tubes, which were also equipped with Kontes greaseless stopcocks. All solvents were dried with appropriate drying agents under a dinitrogen atmosphere and were distilled prior to use, or they were transferred directly under vacuum from the appropriate drying agent. Hydrocarbon solvents, diethyl ether, and tetrahydrofuran were dried and distilled from sodium benzophenone ketyl. Commercially available  $(\text{CH}_2\text{CHCHMe})\text{MgCl}$  (Aldrich, 0.5 M in THF) was transformed into the corresponding diallylmagnesium reagent in the usual manner.<sup>23</sup>  $\text{Cp}^*\text{W}(\text{NO})(\text{CH}_2\text{CMe}_3)\text{Cl}$ <sup>7</sup> and  $\text{Cp}^*\text{W}(\text{NO})(\text{CH}_2\text{CMe}_3)(\eta^3\text{-CH}_2\text{CHCHMe})$  (**1**)<sup>8</sup> were prepared according to the published procedures. The progress of all reactions was monitored by NMR spectroscopy, and this monitoring indicated that no other major organometallic products were formed during the various transformations. The isolated yields of all new complexes have not been optimized.

All IR samples were prepared as Nujol mulls, and their spectra were recorded on a Thermo Nicolet 4700 FT-IR spectrometer. NMR spectra were recorded at room temperature on Bruker AV-300 or AV-400 spectrometers. All chemical shifts are reported in ppm, and all coupling constants are reported in Hz.  $^1\text{H}$  NMR spectra are referenced to the residual protio isotopomer present in a particular solvent, and  $^{13}\text{C}$  NMR spectra are referenced to the natural-abundance carbon signal of the solvent

employed.  $^{31}\text{P}$  NMR spectra are referenced to  $\text{H}_3\text{PO}_4$ . When necessary,  $^1\text{H}$ – $^1\text{H}$  COSY,  $^1\text{H}$ – $^{13}\text{C}$  HSQC,  $^1\text{H}$ – $^{13}\text{C}$  HMBC, and  $^{13}\text{C}$  APT experiments were carried out to correlate and assign  $^1\text{H}$  and  $^{13}\text{C}$  NMR signals. Low- and high-resolution mass spectra (EI, 70 eV) were recorded by the staff of the UBC mass spectrometry facility using a Kratos MS-50 spectrometer. Elemental analyses were performed by Mr. David Wong of the UBC microanalytical facility.

**Preparation of  $\text{Cp}^*\text{W}(\text{NO})(\text{CH}_2\text{CH}_2\text{CH}_2\text{Cl})(\eta^3\text{-CH}_2\text{CHCHMe})$  (**2**).** In a glovebox, **1** (50.0 mg, 0.110 mmol) was dissolved in 1-chloropropane (3 mL) in a 4 dram vial. The mixture was allowed to sit undisturbed for 24 h at room temperature, after which the solvent was removed *in vacuo*. The remaining orange-brown residue was redissolved in pentane (9 mL), and the solution was chromatographed on an alumina column (1 × 4 cm) using 4:1 pentane/ $\text{Et}_2\text{O}$  (20 mL) as the eluant. The yellow band that eluted was collected, and the solvent was removed from the eluate *in vacuo*. Yellow, rod-shaped crystals of **2** were obtained by recrystallizing the yellow residue from a minimal amount of pentane (2 mL) at  $-30^\circ\text{C}$ . Yield: 21 mg (39%).

Characterization data for **2**: IR ( $\text{cm}^{-1}$ ) 1599 (s,  $\nu_{\text{NO}}$ );  $^1\text{H}$  NMR (300 MHz,  $\text{C}_6\text{D}_6$ )  $\delta$  0.78 (m, 1H, chloropropyl  $\text{CH}_2$ ), 0.95 (m, 1H, chloropropyl  $\text{CH}_2$ ), 1.05 (m, 1H, allyl  $\text{CHCH}_3$ ), 1.45 (s, 15H,  $\text{C}_5\text{Me}_5$ ), 1.47 (observed m, 1H, allyl  $\text{CH}_2$ ), 1.65 (m, 1H, chloropropyl  $\text{CH}_2$ ), 1.87 (d,  $^3J_{\text{HH}} = 5.6$ , 3H, allyl  $\text{CH}_3$ ), 2.36 (m, 1H, chloropropyl  $\text{CH}_2$ ), 3.07 (d,  $^3J_{\text{HH}} = 7.1$ , 1H, allyl  $\text{CH}_2$ ), 3.40 (m, 1H,  $\text{CH}_2\text{Cl}$ ), 3.50 (m, 1H,  $\text{CH}_2\text{Cl}$ ), 4.73 (ddd,  $^3J_{\text{HH}} = 13.7$ , 9.3, 7.1, 1H, allyl CH);  $^{13}\text{C}\{^1\text{H}\}$  NMR (75 MHz,  $\text{C}_6\text{D}_6$ )  $\delta$  9.2 ( $\text{C}_5\text{Me}_5$ ), 10.7 ( $\text{WCH}_2$ ), 17.4 (allyl  $\text{CH}_3$ ), 37.4 (chloropropyl  $\text{CH}_2$ ), 51.0 ( $\text{CH}_2\text{Cl}$ ), 54.3 (allyl  $\text{CHCH}_3$ ), 74.6 (allyl  $\text{CH}_2$ ), 105.5 ( $\text{C}_5\text{Me}_5$ ), 109.8 (allyl CH). Anal. Calcd for  $\text{C}_{17}\text{H}_{28}\text{ClNO}$ : C 42.39, H 5.86, N 2.91. Found: C 42.45, H 5.84, N 3.05.

**Preparation of  $\text{Cp}^*\text{W}(\text{NO})(\text{CH}_2(\text{CH}_2)_2\text{CH}_2\text{Cl})(\eta^3\text{-CH}_2\text{CHCHMe})$  (**3**).** In a glovebox, **1** (70.0 mg, 0.147 mmol) was dissolved in 1-chlorobutane (3 mL) in a 4 dram vial. The mixture was allowed to sit undisturbed for 24 h at room temperature, after which the solvent was removed *in vacuo*. The resulting orange-brown residue was redissolved in pentane (9 mL), and the solution was chromatographed on an alumina column (1 × 4 cm) using 4:1 pentane/ $\text{Et}_2\text{O}$  (20 mL) as the eluant. The yellow band that eluted was collected, and the solvent was removed *in vacuo*. Yellow, rod-shaped crystals of **3** were obtained by recrystallizing the yellow residue from a minimal amount of pentane (2 mL) at  $-30^\circ\text{C}$ . Yield: 20 mg (36%).

Characterization data for **3**: IR ( $\text{cm}^{-1}$ ) 1599 (s,  $\nu_{\text{NO}}$ );  $^1\text{H}$  NMR (300 MHz,  $\text{C}_6\text{D}_6$ )  $\delta$  0.88 (m, 2H, chlorobutyl  $\text{CH}_2$ ), 1.09 (m, 1H, allyl  $\text{CHCH}_3$ ), 1.27 (m, 1H, chlorobutyl  $\text{CH}_2$ ), 1.82 (observed m, 2H, chlorobutyl  $\text{CH}_2$ ), 2.42 (m, 1H, chlorobutyl  $\text{CH}_2$ ), 1.48 (s, 15H,  $\text{C}_5\text{Me}_5$ ), 1.91 (d,  $^3J_{\text{HH}} = 5.9$ , 3H, allyl  $\text{CH}_3$ ), 3.19 (d,  $^3J_{\text{HH}} = 7.2$ , 1H, allyl  $\text{CH}_2$ ), 3.35 (m, H,  $\text{CH}_2\text{Cl}$ ), 3.43 (m, 1H,  $\text{CH}_2\text{Cl}$ ), 4.84 (ddd,  $^3J_{\text{HH}} = 13.7$ , 9.0, 7.2, 1H, allyl CH);  $^{13}\text{C}\{^1\text{H}\}$  NMR (75 MHz,  $\text{C}_6\text{D}_6$ )  $\delta$  9.8 ( $\text{C}_5\text{Me}_5$ ), 14.8 ( $\text{WCH}_2$ ), 18.0 (allyl  $\text{CH}_3$ ), 31.7 (chlorobutyl  $\text{CH}_2$ ), 40.6 (chlorobutyl  $\text{CH}_2$ ), 45.5 ( $\text{CH}_2\text{Cl}$ ), 54.7 (allyl  $\text{CHCH}_3$ ), 74.8 (allyl  $\text{CH}_2$ ), 106.0 ( $\text{C}_5\text{Me}_5$ ), 110.2 (allyl CH). Anal. Calcd for  $\text{C}_{18}\text{H}_{30}\text{ClNO}$ : C 43.61, H 6.10, N 2.83. Found: C 43.99, H 6.10, N 2.81.

**Preparation of  $\text{Cp}^*\text{W}(\text{NO})(\text{CH}_2(\text{CH}_2)_2\text{CH}_2\text{Br})(\eta^3\text{-CH}_2\text{CHCHMe})$  (**4**).** The preparation of this compound was effected in a manner identical to that described in the previous two sections for the reactions of  $\text{Cp}^*\text{W}(\text{NO})(\text{CH}_2\text{CMe}_3)(\eta^3\text{-CH}_2\text{CHCHMe})$  (**1**) with the analogous 1-chloroalkanes.

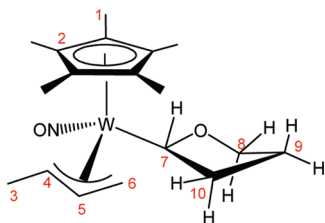
Characterization data for **4**: IR ( $\text{cm}^{-1}$ ) 1597 (s,  $\nu_{\text{NO}}$ );  $^1\text{H}$  NMR (300 MHz,  $\text{C}_6\text{D}_6$ )  $\delta$  0.86 (m, 2H, bromobutyl  $\text{CH}_2$ ), 1.05 (m, 1H, allyl  $\text{CHCH}_3$ ), 1.27 (m, 1H, bromobutyl  $\text{CH}_2$ ), 1.82 (observed m, 2H, bromobutyl  $\text{CH}_2$ ), 2.42 (m, 1H, bromobutyl  $\text{CH}_2$ ), 1.47 (s, 15H,  $\text{C}_5\text{Me}_5$ ), 1.91 (d,  $^3J_{\text{HH}} = 5.8$ , 3H, allyl  $\text{CH}_3$ ), 3.20 (m, 1H,  $\text{CH}_2\text{Br}$ ), 3.27 (m, 1H,  $\text{CH}_2\text{Br}$ ), 4.86 (ddd,  $^3J_{\text{HH}} = 13.7$ , 9.2, 7.2, 1H, allyl CH);  $^{13}\text{C}\{^1\text{H}\}$  NMR (75 MHz,  $\text{C}_6\text{D}_6$ )  $\delta$  9.2 ( $\text{C}_5\text{Me}_5$ ), 15.3 ( $\text{WCH}_2$ ), 17.4 (allyl  $\text{CH}_3$ ), 32.4 (bromobutyl

CH<sub>2</sub>), 33.9 (bromobutyl CH<sub>2</sub>), 40.2 (CH<sub>2</sub>Br), 54.1 (allyl CHCH<sub>3</sub>), 74.2 (allyl CH<sub>2</sub>), 105.3 (C<sub>5</sub>Me<sub>5</sub>), 109.6 (allyl CH); MS (LREI, *m/z*, probe temperature 150 °C) 540 [M<sup>+</sup>].

**Preparation of Cp\*W(NO)((CH<sub>2</sub>)<sub>4</sub>O(CH<sub>2</sub>)<sub>3</sub>CH<sub>3</sub>)(η<sup>3</sup>-CH<sub>2</sub>-CHCHMe) (5).** In a glovebox, **1** (116 mg, 0.244 mmol) was dissolved in di-*n*-butyl ether (1 mL) in a 4 dram vial to obtain a yellow solution. The solution was stirred for 24 h at room temperature, after which the solvent was removed *in vacuo*. The resulting dark brown residue was redissolved in pentane (1.5 mL), and the solution was transferred to the top of an alumina column (1 × 4 cm). The column was eluted with a 1:1 pentane/Et<sub>2</sub>O mixture (10 mL). The yellow band that developed was collected, and the solvent was removed from the eluate *in vacuo* to obtain **5** as a pale yellow solid (94 mg, 81%). This solid was dissolved in a minimum of Et<sub>2</sub>O (0.5 mL), and the solution was stored overnight at −30 °C to induce the deposition of colorless crystals of **5**.

Characterization data for **5**: IR (cm<sup>−1</sup>) 1598 (s, ν<sub>NO</sub>); <sup>1</sup>H NMR (300 MHz, C<sub>6</sub>D<sub>6</sub>) δ 0.89 (t, <sup>3</sup>J<sub>HH</sub> = 7.3, 3H, ether CH<sub>3</sub>), 1.06 (m, 2H, ether CH<sub>2</sub>), 1.12 (m, 1H, CH<sub>2</sub>CHCHMe), 1.41 (m, 2H, ether CH<sub>2</sub>), 1.50 (s, 15H, C<sub>5</sub>Me<sub>5</sub>), 1.52 (s, 1H, CH<sub>2</sub>-CHCHMe), 1.62 (m, 2H, ether CH<sub>2</sub>), 1.88 (observed m, 2H, ether CH<sub>2</sub>), 1.91 (d, <sup>3</sup>J<sub>HH</sub> = 5.5, 3H, CH<sub>2</sub>CHCHMe), 2.07 (m, 2H, ether CH<sub>2</sub>), 3.26 (d, <sup>2</sup>J<sub>HH</sub> = 7.3, 1H, CH<sub>2</sub>CHCHMe), 3.37 (t, <sup>3</sup>J<sub>HH</sub> = 6.4, 2H, ether OCH<sub>2</sub>), 3.53 (m, 2H, ether OCH<sub>2</sub>), 4.90 (ddd, <sup>3</sup>J<sub>HH</sub> = 13.7, 9.4, 7.3, CH<sub>2</sub>CHCHMe); <sup>13</sup>C{<sup>1</sup>H} NMR (100 MHz, C<sub>6</sub>D<sub>6</sub>) δ 10.1 (C<sub>5</sub>Me<sub>5</sub>), 14.9 (ether Me), 16.6 (ether CH<sub>2</sub>), 18.3 (CH<sub>2</sub>CHCHMe), 20.6 (ether CH<sub>2</sub>), 31.5 (ether CH<sub>2</sub>), 33.2 (ether CH<sub>2</sub>), 38.5 (ether CH<sub>2</sub>), 54.9 (CH<sub>2</sub>CHCHMe), 71.4 (ether OCH<sub>2</sub>), 72.0 (ether OCH<sub>2</sub>), 75.2 (CH<sub>2</sub>CHCHMe), 106.2 (C<sub>5</sub>Me<sub>5</sub>), 110.3 (CH<sub>2</sub>CHCHMe); MS (LREI, *m/z*, probe temperature 150 °C) 533 [M<sup>+</sup>].

**Preparation of Cp\*W(NO)(C<sub>4</sub>H<sub>7</sub>O)(η<sup>3</sup>-MeCHCHCH<sub>2</sub>) (6).** In a glovebox, **1** (105 mg, 0.221 mmol) was dissolved in THF (1 mL) in a 4 dram vial to obtain an orange-yellow solution. The solution was stirred for 24 h at room temperature, after which the solvent was removed *in vacuo*. The resulting dark brown residue was redissolved in a 1:1 pentane/Et<sub>2</sub>O mixture (1.5 mL), and the solution was transferred to the top of an alumina column (1 × 4 cm). The column was eluted with a 1:1 pentane/Et<sub>2</sub>O mixture (10 mL). The yellow band that developed was collected, and the solvent was removed from the eluate *in vacuo* to obtain **6** as a yellow solid (40 mg, 38%). This solid was dissolved in a minimum of Et<sub>2</sub>O (0.5 mL), and the solution was stored overnight at −30 °C to induce the deposition of X-ray quality yellow crystals of **6**.



Characterization data for **6**: IR (Nujol, cm<sup>−1</sup>) 1602 (s, ν<sub>NO</sub>). <sup>1</sup>H NMR (300 MHz, C<sub>6</sub>D<sub>6</sub>) δ 1.36 (m, 1H, C(4)H<sub>2</sub>), 1.49 (m, 1H, C(10)H<sub>2</sub>), 1.62 (overlapping m, 2H, C(9)H<sub>2</sub>), 1.68 (s, 15H, C<sub>5</sub>Me<sub>5</sub>), 1.95 (d, <sup>2</sup>J<sub>HH</sub> = 5.8, 3H, C(3)H<sub>3</sub>), 2.47 (m, 1H, C(10)H<sub>2</sub>), 3.42 (obs, 1H, C(8)H<sub>2</sub>), 3.44 (d, <sup>2</sup>J<sub>HH</sub> = 7.1, 1H, C(6)H<sub>2</sub>), 3.84 (m, 1H, C(6)H<sub>2</sub>), 4.04 (dd, <sup>3</sup>J<sub>HH</sub> = 11.0, 5.2, 1H, C(7)H), 4.94 (ddd, <sup>3</sup>J<sub>HH</sub> = 13.9, 9.1, 7.1, 1H, C(5)H). <sup>13</sup>C APT NMR (100 MHz, C<sub>6</sub>D<sub>6</sub>) δ 10.3 (C<sub>5</sub>Me<sub>5</sub>), 18.3 (C3), 28.1 (C9), 36.5 (C10), 57.8 (C4), 70.3 (C8), 74.1 (C6), 78.9 (C7), 107.6 (C<sub>5</sub>Me<sub>5</sub>), 112.1 (C5). MS (LREI, *m/z*, probe temperature 120 °C) 475 [M<sup>+</sup>, <sup>184</sup>W].

**Preparation of Cp\*W(NO)(CH<sub>2</sub>CH<sub>2</sub>C<sub>6</sub>H<sub>11</sub>)(η<sup>3</sup>-CH<sub>2</sub>CHCHMe) (7).** In a glovebox, complex **1** (60 mg, 0.13 mmol) was dissolved in ethylcyclohexane (3 mL) in a 4 dram vial. The mixture was allowed to sit undisturbed for 24 h at room temperature, after which time the

solvent was removed *in vacuo*. The remaining brown residue was redissolved in pentane (9 mL), and the solution was chromatographed on an alumina column (1 × 4 cm) using 2:1 pentane/Et<sub>2</sub>O (10 mL) as the eluant. The yellow band that eluted was collected, and the solvent was removed from the eluate *in vacuo*. Blocks of yellow crystals of **7** were obtained by recrystallizing the yellow residue from a minimal amount of 4:1 pentane/Et<sub>2</sub>O (2 mL) at −30 °C. Yield: 52 mg (82%).

Characterization data for **7**: IR (cm<sup>−1</sup>) 1598 (s, ν<sub>NO</sub>); <sup>1</sup>H NMR (300 MHz, C<sub>6</sub>D<sub>6</sub>) δ 1.04 (m, 2H, cyclohexyl CH<sub>2</sub>), 1.05 (m, 1H, allyl CHCH<sub>3</sub>), 1.06 (m, 2H, WCH<sub>2</sub>), 1.16 (m, 1H, cyclohexyl CH<sub>2</sub>), 1.25 (m, 1H, ethyl CH<sub>2</sub>), 1.32 (observed m, 2H, cyclohexyl CH<sub>2</sub>), 1.33 (m, 1H, cyclohexyl CH), 1.45 (s, 15H, C<sub>5</sub>Me<sub>5</sub>), 1.67 (m, 2H, cyclohexyl CH<sub>2</sub>), 1.81 (m, 1H, cyclohexyl CH<sub>2</sub>), 1.87 (d, <sup>3</sup>J<sub>HH</sub> = 5.9, 3H, allyl CH<sub>3</sub>), 1.99 (m, 1H, ethyl CH<sub>2</sub>), 2.04 (m, 2H, cyclohexyl CH<sub>2</sub>), 3.07 (d, <sup>3</sup>J<sub>HH</sub> = 7.3, 1H, allyl CH<sub>2</sub>), 4.73 (ddd, <sup>3</sup>J<sub>HH</sub> = 13.5, 9.4, 7.3, 1H, allyl CH); <sup>13</sup>C{<sup>1</sup>H} NMR (75 MHz, C<sub>6</sub>D<sub>6</sub>) δ 9.2 (C<sub>5</sub>Me<sub>5</sub>), 12.8 (WCH<sub>2</sub>), 17.5 (allyl CH<sub>3</sub>), 27.1, 27.3, 33.6, 33.7 (cyclohexyl CH<sub>2</sub>), 41.9 (ethyl CH<sub>2</sub>), 44.3 (cyclohexyl CH), 53.9 (allyl CHCH<sub>3</sub>), 74.6 (allyl CH<sub>2</sub>), 105.3 (C<sub>5</sub>Me<sub>5</sub>), 109.2 (allyl CH). Anal. Calcd for C<sub>22</sub>H<sub>37</sub>NOW: C 51.27, H 7.24, N 2.72. Found: C 51.37, H 7.38, N 3.13.

**Preparation of Cp\*Mo(NO)(CH<sub>2</sub>CMe<sub>3</sub>)(η<sup>3</sup>-C<sub>3</sub>H<sub>5</sub>) (8).** Cp\*Mo(NO)Cl<sub>2</sub> (0.76 g, 2.3 mmol) partially dissolved in THF (40 mL) to obtain an orange suspension. A separate Schlenk flask was charged with Mg(CH<sub>2</sub>CMe<sub>3</sub>)<sub>2</sub>·x(dioxane) in THF solution (0.72 mL, titer: 301 mL/mol CH<sub>2</sub>CMe<sub>3</sub>) and additional THF (5 mL). The latter solution was frozen at −196 °C under a flow of dinitrogen, and the orange suspension was cannulated dropwise onto the colorless solution over 30 min. The resulting mixture was allowed to warm to room temperature while being stirred over 1 h. Volatiles were removed from the final brown solution *in vacuo*, and the brown residue was redissolved in Et<sub>2</sub>O (10 mL) to obtain a brown solution. A separate Schlenk flask was charged with Mg(C<sub>3</sub>H<sub>5</sub>)<sub>2</sub>·x(dioxane) (0.272 g, titer: 111 g/mol C<sub>3</sub>H<sub>5</sub>) and Et<sub>2</sub>O (5 mL) to obtain a colorless solution. The latter solution was frozen at −196 °C under a flow of dinitrogen, and the brown solution was cannulated dropwise onto the frozen colorless solid over a period of 30 min. The resulting mixture became brown-purple after warming to room temperature while being stirred over 1 h. The volatiles were then removed *in vacuo*, the resulting brown solid was redissolved in 4:1 pentane/Et<sub>2</sub>O, and this solution was transferred onto a silica column (2 × 6 cm). Elution of the column with pentane developed a peach-colored band, which was eluted and collected. Removal of solvent from the eluate *in vacuo* afforded **8** as a yellow-orange solid (0.16 g, 19%). Recrystallization of this solid from a 1:1 mixture of MeCN/Et<sub>2</sub>O at −30 °C overnight produced orange single crystals of **8**.

Characterization data for **8**: IR (cm<sup>−1</sup>) 1613 (s, ν<sub>NO</sub>); <sup>1</sup>H NMR (300 MHz, C<sub>6</sub>D<sub>6</sub>) δ 0.69 (d, <sup>3</sup>J<sub>HH</sub> = 10.5, 1H, CH<sub>2</sub>CHCH<sub>2</sub>), 1.04 (d, <sup>2</sup>J<sub>HH</sub> = 11.4, 1H, CH<sub>2</sub>CMe<sub>3</sub>), 1.26 (s, 9H, CH<sub>2</sub>-CMe<sub>3</sub>), 1.46 (s, 15H, C<sub>5</sub>Me<sub>5</sub>), 1.75 (d, <sup>2</sup>J<sub>HH</sub> = 11.4, 1H, CH<sub>2</sub>-CMe<sub>3</sub>), 1.78 (d, <sup>3</sup>J<sub>HH</sub> = 14.6, 1H, CH<sub>2</sub>CHCH<sub>2</sub>), 2.46 (d, <sup>3</sup>J<sub>HH</sub> = 3.5, 1H, CH<sub>2</sub>CHCH<sub>2</sub>), 3.86 (d, <sup>3</sup>J<sub>HH</sub> = 3.8, 1H, CH<sub>2</sub>CHCH<sub>2</sub>), 4.99 (m, 1H, allyl CH); <sup>13</sup>C{<sup>1</sup>H} NMR (100 MHz, C<sub>6</sub>D<sub>6</sub>) δ 10.3 (C<sub>5</sub>Me<sub>5</sub>), 34.2 (CH<sub>2</sub>CMe<sub>3</sub>), 34.8 (CH<sub>2</sub>CMe<sub>3</sub>), 39.2 (CH<sub>2</sub>CMe<sub>3</sub>), 46.6 (allyl CH<sub>2</sub>), 83.6 (allyl CH<sub>2</sub>), 107.8 (C<sub>5</sub>Me<sub>5</sub>), 112.8 (allyl CH); MS (LREI, *m/z*, probe temperature 120 °C) 375 [M<sup>+</sup>]. Anal. Calcd for C<sub>18</sub>H<sub>31</sub>MoNO: C, 57.90; H, 8.37; N, 3.75. Found: C, 57.56; H, 8.32; N, 3.78.

**Preparation of Cp\*Mo(NO)(C<sub>5</sub>H<sub>5</sub>N)(η<sup>2</sup>-CH<sub>2</sub>=CHCH<sub>2</sub>CH<sub>2</sub>-*t*-Bu) (9).** A thick-walled reaction vessel was charged with Cp\*Mo(NO)(CH<sub>2</sub>CMe<sub>3</sub>)(C<sub>3</sub>H<sub>5</sub>) (**8**) (104 mg, 0.279 mmol), pyridine (0.05 mL, 0.6 mmol, 2 equiv), and benzene (5 mL). The yellow solution was maintained at 35 °C for 3 days, and then the solvent was removed *in vacuo* to obtain an oily, orange residue. Cooling of this residue to −30 °C overnight induced the precipitation of **9** (47 mg, 37%), which was collected and washed



with  $2 \times 0.5$  mL of cold pentane. Crystals of **9** suitable for an X-ray crystallographic analysis were grown from a saturated pentane solution maintained at  $-30$  °C.

Characterization data for **9**: IR ( $\text{cm}^{-1}$ ) 1553 (m,  $\nu_{\text{NO}}$ );  $^1\text{H}$  NMR (300 MHz,  $\text{C}_6\text{D}_6$ )  $\delta$  0.85 (m, 1H,  $\text{CH}_2=\text{CHCH}_2$ ), 1.12 (s, 9H,  $\text{CH}_2\text{CMe}_3$ ), 1.60 (s, 15H,  $\text{C}_5\text{Me}_5$ ), 1.79 (m, 2H,  $\text{CH}_2\text{CMe}_3$ ), 2.21 (m, 1H,  $\text{CH}_2=\text{CHCH}_2$ ), 2.30 (observed, 1H,  $\text{CH}_2=\text{CHCH}_2$ ), 2.34 (m, 1H,  $\text{CH}_2=\text{CHCH}_2$ ), 2.57 (m, 1H,  $\text{CH}_2=\text{CHCH}_2$ ), 6.28 (m, 2H, pyridine CH), 6.65 (tt, 1H, pyridine CH), 8.48 (m, 2H, pyridine CH);  $^{13}\text{C}\{^1\text{H}\}$  NMR (100 MHz,  $\text{C}_6\text{D}_6$ )  $\delta$  10.1 ( $\text{C}_5\text{Me}_5$ ), 30.3 ( $\text{CH}_2\text{CMe}_3$ ), 31.3 ( $\text{CH}_2\text{CMe}_3$ ), 36.1 ( $\text{CH}_2=\text{CHCH}_2$ ), 49.8 ( $\text{CH}_2\text{CMe}_3$ ), 51.6 ( $\text{CH}_2=\text{CHCH}_2$ ), 68.6 ( $\text{CH}_2=\text{CHCH}_2$ ), 104.9 ( $\text{C}_5\text{Me}_5$ ), 124.2 (pyridine CH), 136.0 (pyridine CH), 155.4 (pyridine CH); MS (LREI,  $m/z$ , probe temperature 100 °C) 452 [ $\text{M}^+$ ]; (HREI,  $m/z$ ,  $^{98}\text{Mo}$ ) theoretical 454.18817, found 454.18830.

**Preparation of  $\text{Cp}^*\text{Mo}(\text{NO})(\text{PMe}_3)(\eta^2\text{-CH}_2=\text{CHCH}_2\text{CH}_2\text{-t-Bu})$  (**10**).** A thick-walled reaction vessel was charged with **8** (112 mg, 0.300 mmol),  $\text{PMe}_3$  (0.05 mL, 0.6 mmol, 2 equiv), and benzene (5 mL). The yellow solution was heated at 35 °C for 3 days, after which time the solvent was removed *in vacuo* to obtain **10** as a dark brown oil (130 mg, 96%).

Characterization data for **10**: IR ( $\text{cm}^{-1}$ ) 1573 (m,  $\nu_{\text{NO}}$ );  $^1\text{H}$  NMR (400 MHz,  $\text{C}_6\text{D}_6$ )  $\delta$  0.30 (ddd, 1H,  $^2J_{\text{HH}} = 9.7$ ,  $^3J_{\text{HH}} = 7.3$ ,  $^4J_{\text{HH}} = 3.8$ ,  $\text{CH}_2=\text{CHCH}_2$ ), 1.06 (s, 9H,  $\text{CH}_2\text{CMe}_3$ ), 1.13 (d, 9H,  $^2J_{\text{PH}} = 8.1$ ,  $\text{PMe}_3$ ), 1.38 (ddd, 1H,  $^3J_{\text{HH}} = 13.0$ ,  $^2J_{\text{HH}} = 9.3$ ,  $^4J_{\text{HH}} = 4.0$ ,  $\text{CH}_2=\text{CHCH}_2$ ), 1.64 (observed, 1H,  $\text{CH}_2=\text{CHCH}_2$ ) 1.68 (s, 15H,  $\text{C}_5\text{Me}_5$ ), 1.75 (m, 2H,  $\text{CH}_2=\text{CHCH}_2$ ), 1.91 (m, 1H,  $\text{CH}_2\text{CMe}_3$ ), 2.07 (m, 1H,  $\text{CH}_2\text{CMe}_3$ );  $^{13}\text{C}\{^1\text{H}\}$  NMR (100 MHz,  $\text{C}_6\text{D}_6$ )  $\delta$  10.9 ( $\text{C}_5\text{Me}_5$ ), 17.2 (d,  $^1J_{\text{CP}} = 27.6$ ,  $\text{PMe}_3$ ), 30.4 ( $\text{CH}_2\text{CMe}_3$ ), 31.2 ( $\text{CH}_2\text{CMe}_3$ ), 35.3 ( $\text{CH}_2\text{CMe}_3$ ), 38.5 (d,  $^2J_{\text{CP}} = 11.0$ ,  $\text{CH}_2=\text{CHCH}_2$ ), 49.6 ( $\text{CH}_2=\text{CHCH}_2$ ), 53.7 ( $\text{CH}_2=\text{CHCH}_2$ ), 104.2 ( $\text{C}_5\text{Me}_5$ );  $^{31}\text{P}\{^1\text{H}\}$  NMR (121.5 MHz,  $\text{C}_6\text{D}_6$ )  $\delta$  20.6 ( $\text{PMe}_3$ ); MS (LREI,  $m/z$ , probe temperature 100 °C) 451 [ $\text{M}^+$ ]; (HREI,  $m/z$ ,  $^{98}\text{Mo}$ ) theoretical 451.19016, found 451.19050.

**Preparation of  $\text{Cp}^*\text{Mo}(\text{NO})(\text{CH}_2\text{SiMe}_3)(\eta^3\text{-CH}_2\text{CHCHMe})$  (**11**).** A Schlenk flask maintained at  $-196$  °C with a liquid  $\text{N}_2$  bath was charged with  $\text{Cp}^*\text{Mo}(\text{NO})\text{Cl}_2$  (0.50 g, 1.5 mmol),  $\text{Mg}(\text{CH}_2\text{SiMe}_3)_2 \cdot x(\text{dioxane})$  (0.30 g, titer: 190 g/mol  $\text{CH}_2\text{SiMe}_3$ ), and THF (60 mL). While being stirred over 2 h, the dark orange mixture was first allowed to warm to  $-70$  °C, whereupon it became green-brown, then to room temperature, whereupon it became indigo in color. Removal of the solvent from the final mixture *in vacuo* left a dark indigo residue, which was redissolved in  $\text{Et}_2\text{O}$  (25 mL). In a separate Schlenk flask,  $\text{Mg}(\text{CH}_2\text{CHCHMe})_2 \cdot x(\text{dioxane})$  (0.17 g, titer: 112 g/mol  $\text{CH}_2\text{CHCHMe}$ ) was dissolved in  $\text{Et}_2\text{O}$  (10 mL) to obtain a colorless solution. This solution was frozen at  $-196$  °C, and the indigo solution was added to it dropwise over a period of 30 min. The resulting mixture became reddish-purple while being stirred and was allowed to warm to room temperature over 1 h. The volatiles were removed from the final mixture *in vacuo*, the residual purple-red solid was dissolved in 4:1 pentane/ $\text{Et}_2\text{O}$ , and the solution was transferred onto a silica column ( $2 \times 8$  cm). Elution of the column with a mixture of 4:1 pentane/ $\text{Et}_2\text{O}$  produced a magenta eluate, which was collected. Removal of solvent from the eluate *in vacuo* afforded **11** (0.24 g, 39%) as a reddish-purple solid.

Characterization data for **11**: IR ( $\text{cm}^{-1}$ ) 1609 (s,  $\nu_{\text{NO}}$ );  $^1\text{H}$  NMR (300 MHz,  $\text{C}_6\text{D}_6$ )  $\delta$  (major isomer)  $-0.54$  (d, 1H,  $^2J_{\text{HH}} = 11.4$ ,  $\text{CH}_2\text{SiMe}_3$ ),  $-0.01$  (d, 1H,  $^2J_{\text{HH}} = 11.4$ ,  $\text{CH}_2\text{SiMe}_3$ ), 0.34 (s, 9H,  $\text{CH}_2\text{SiMe}_3$ ), 1.45 (s, 15H,  $\text{C}_5\text{Me}_5$ ), 1.50 (d, obscured,  $\text{MeCHCHCH}_2$ ), 1.60 (s, 3H,  $\text{MeCHCHCH}_2$ ), 1.85 (d,  $^2J_{\text{HH}} = 10.2$ , 1H,  $\text{MeCHCHCH}_2$ ), 3.45 (d,  $^3J_{\text{HH}} = 7.6$ , 1H,  $\text{MeCHCHCH}_2$ ), 4.96 (ddd,  $^3J_{\text{HH}} = 14.2$ , 10.0, 7.6, 1H,  $\text{MeCHCHCH}_2$ );  $\delta$  (minor isomer, selected peaks)  $-0.70$  (d, 1H,  $^2J_{\text{HH}} = 12.6$ ,  $\text{CH}_2\text{SiMe}_3$ ),  $-0.40$  (d, 1H,  $^2J_{\text{HH}} = 12.6$ ,  $\text{CH}_2\text{SiMe}_3$ ), 0.35 (s, 9H,  $\text{CH}_2\text{SiMe}_3$ ), 1.46 (s, 15H,  $\text{C}_5\text{Me}_5$ ), 4.64 (m, 1H,  $\text{MeCHCHCH}_2$ ); MS (LREI,  $m/z$ , probe temperature 120 °C) 405 [ $\text{M}^+$ ].

**Preparation of  $\text{Cp}^*\text{Mo}(\text{NO})(\eta^2\text{-CH}_2=\text{CHCH}=\text{CH}_2)(\text{PMe}_3)$  (**12**).** In a glovebox, complex **11** (30 mg, 0.07 mmol) was dissolved in  $\text{PMe}_3$  (0.5 mL) to obtain a red-orange solution, which was stored for 18 h at room temperature. Volatiles were removed from the final mixture *in vacuo* to obtain a light brown solid, which was redissolved in a mixture of 1:2 pentane/ $\text{Et}_2\text{O}$ , then transferred onto a silica column ( $1 \times 4$  cm). Upon elution of the column with  $\text{Et}_2\text{O}$ , an orange band developed and was collected. Solvent was removed from the eluate *in vacuo* to obtain **12** as an amorphous, orange solid (11 mg, 38%).

Characterization data for **12**: IR ( $\text{cm}^{-1}$ ) 1578 (s,  $\nu_{\text{NO}}$ );  $^1\text{H}$  NMR (400 MHz,  $\text{C}_6\text{D}_6$ )  $\delta$  0.50 (m, 1H, metal-bound  $\text{H}_2\text{C}=\text{CH}$ ), 1.06 (d, 9H,  $^2J_{\text{HP}} = 7.9$ ,  $\text{PMe}_3$ ), 1.59 (d, 1H,  $^3J_{\text{HH}} = 3.1$ , metal-bound  $\text{H}_2\text{C}=\text{CH}$ ), 1.63 (s, 15H,  $\text{C}_5\text{Me}_5$ ), 2.30 (m, 1H, metal-bound  $\text{H}_2\text{C}=\text{CH}$ ), 4.73 (dd, 1H,  $^2J_{\text{HH}} = 10.1$ ,  $^3J_{\text{HH}} = 2.2$ , uncoordinated  $\text{H}_2\text{C}=\text{CH}$ ), 5.23 (dd, 1H,  $^2J_{\text{HH}} = 16.6$ ,  $^3J_{\text{HH}} = 2.2$ , uncoordinated  $\text{H}_2\text{C}=\text{CH}$ ), 5.98 (dt, 1H,  $^3J_{\text{HH}} = 17.0$ , 9.9, uncoordinated  $\text{H}_2\text{C}=\text{CH}$ );  $^{13}\text{C}\{^1\text{H}\}$  NMR (100 MHz,  $\text{C}_6\text{D}_6$ )  $\delta$  10.2 ( $\text{C}_5\text{Me}_5$ ), 17.1 (d,  $^1J_{\text{CP}} = 27.0$ ,  $\text{PMe}_3$ ), 38.1 (d,  $^2J_{\text{CP}} = 11.0$ , metal-bound  $\text{H}_2\text{C}=\text{CH}$ ), 52.6 (metal-bound  $\text{H}_2\text{C}=\text{CH}$ ), 102.3 (uncoordinated  $\text{H}_2\text{C}=\text{CH}$ ), 104.6 ( $\text{C}_5\text{Me}_5$ ), 148.7 (uncoordinated  $\text{H}_2\text{C}=\text{CH}$ ); MS (LREI,  $m/z$ , probe temperature 120 °C) 393 [ $\text{M}^+$ ]; (HREI,  $m/z$ ,  $^{98}\text{Mo}$ ) theoretical 393.11191, found 393.11203.

**Preparation of  $\text{Cp}^*\text{Mo}(\text{NO})(\eta^4\text{-trans-CH}_2=\text{CHCH}=\text{CH}_2)$  (**13**).** In a glovebox, complex **11** (246 mg, 0.61 mmol) was dissolved in pentane, and the solution was stored for 18 h at room temperature. The mixture was then taken to dryness *in vacuo*, the remaining black residue was redissolved in a mixture of 4:1 pentane/ $\text{Et}_2\text{O}$ , and the solution was transferred onto an alumina column ( $1.5 \times 5$  cm). Elution of the column with a mixture of 4:1 pentane/ $\text{Et}_2\text{O}$  produced a peach-colored band, which was collected. Solvent was removed from the eluate *in vacuo*, and the residual yellow-orange solid was recrystallized from pentane at  $-30$  °C to obtain **13** as yellow-orange crystals (68 mg, 35%).

Characterization data for **13**: IR ( $\text{cm}^{-1}$ ) 1607 (s,  $\nu_{\text{NO}}$ );  $^1\text{H}$  NMR (400 MHz,  $\text{C}_6\text{D}_6$ )  $\delta$  1.15 (dd, 1H,  $^2J_{\text{HH}} = 12.3$ ,  $^3J_{\text{HH}} = 2.2$ ,  $\text{CH}_2\text{CHCHCH}_2$ ), 1.51 (m, 1H,  $\text{CH}_2\text{CHCHCH}_2$ ), 1.59 (s, 15H,  $\text{C}_5\text{Me}_5$ ), 2.38 (dd, 1H,  $^2J_{\text{HH}} = 6.7$ ,  $^3J_{\text{HH}} = 2.0$ ,  $\text{CH}_2\text{CHCHCH}_2$ ), 3.01 (dd, 1H,  $^2J_{\text{HH}} = 13.9$ ,  $^3J_{\text{HH}} = 2.2$ ,  $\text{CH}_2\text{CHCHCH}_2$ ), 3.41 (m, 1H,  $\text{CH}_2\text{CHCHCH}_2$ ), 3.53 (ddd, 1H,  $^3J_{\text{HH}} = 12.6$ , 10.7, 6.1,  $\text{CH}_2\text{CHCHCH}_2$ );  $^{13}\text{C}\{^1\text{H}\}$  NMR (100 MHz,  $\text{C}_6\text{D}_6$ )  $\delta$  10.5 ( $\text{C}_5\text{Me}_5$ ), 58.9 ( $\text{CH}_2\text{CHCHCH}_2$ ), 61.4 ( $\text{CH}_2\text{CHCHCH}_2$ ), 91.2 ( $\text{CH}_2\text{CHCHCH}_2$ ), 96.0 ( $\text{CH}_2\text{CHCHCH}_2$ ), 105.6 ( $\text{C}_5\text{Me}_5$ ); MS (LREI,  $m/z$ , probe temperature 120 °C) 371 [ $\text{M}^+$ ]. Anal. Calcd for  $\text{C}_{14}\text{H}_{21}\text{MoNO}$ : C, 53.34; H, 6.71; N, 4.44. Found: C, 53.52; H, 6.78; N, 4.50.

**Monitoring the Conversion of **11** to **13**.** In a glovebox, complex **11** (22 mg, 0.054 mmol) was dissolved in pentane (0.8 mL) and transferred to a J. Young NMR tube equipped with a Kontes greaseless stopcock and a capillary containing  $\text{C}_6\text{D}_6$ . The sample was stored at 20 °C under a  $\text{N}_2$  atmosphere, and its  $^1\text{H}$  NMR spectrum was recorded periodically. The area under the signal at  $-0.70$  ppm (d, 1H,  $\text{CH}_2\text{SiMe}_3$ ) was integrated against the signal at 7.16 ppm corresponding to the residual protio isotopomer of  $\text{C}_6\text{D}_6$ .

**X-ray Crystallography.** Data collection was carried out at  $-170 \pm 2$  °C on a Bruker X8 or DUO APEX diffractometer, using graphite-monochromated Mo K $\alpha$  radiation.

Data for **3** were collected to a maximum  $2\theta$  value of  $56.3^\circ$  in  $0.5^\circ$  oscillations. The structure was solved by direct methods<sup>24</sup> and expanded using Fourier techniques. All non-hydrogen atoms were refined anisotropically, and all hydrogen atoms were included in fixed positions. The final cycle of full-matrix least-squares analysis was based on 4553 observed reflections and 221 variable parameters.

(24) SIR-92: Altomare, A.; Cascarano, G.; Giacovazzo, C.; Guagliardi, A. *J. Appl. Crystallogr.* **1993**, *26*, 343.



Table 3. X-ray Crystallographic Data for Complexes 3, 5, 6, 8, 9, and 13

	3	5	6
Crystal Data			
empirical formula	C <sub>18</sub> H <sub>30</sub> ClNO <sub>2</sub>	C <sub>22</sub> H <sub>39</sub> NO <sub>2</sub>	C <sub>18</sub> H <sub>29</sub> NO <sub>2</sub>
cryst habit, color	needle, yellow	needle, colorless	needle, yellow
cryst size (mm)	0.30 × 0.16 × 0.16	0.33 × 0.16 × 0.14	0.40 × 0.10 × 0.05
cryst syst	monoclinic	monoclinic	orthorhombic
space group	<i>P</i> 2 <sub>1</sub> / <i>c</i>	<i>P</i> 2 <sub>1</sub> / <i>n</i>	<i>F</i> dd2
volume (Å <sup>3</sup> )	1863.8(2)	2219.4(2)	7257.5(3)
<i>a</i> (Å)	14.2503(9)	9.0160(6)	26.6043(6)
<i>b</i> (Å)	7.9664(5)	16.5990(11)	29.9393(6)
<i>c</i> (Å)	17.0315(11)	14.8412(9)	9.1116(2)
α (deg)	90	90	90
β (deg)	105.432(2)	92.2480(10)	90
γ (deg)	90	90	90
<i>Z</i>	4	4	16
density (calcd) (Mg/m <sup>3</sup> )	1.767	1.596	1.740
absorp coeff (mm <sup>-1</sup> )	6.343	5.220	6.373
<i>F</i> <sub>000</sub>	976	1072	3744
Data Collection and Refinement			
measd reflns: total	17 888	38 070	11 532
measd reflns: unique	4553	6505	3854
final <i>R</i> indices <sup>a</sup>	<i>R</i> 1 = 0.0204, <i>wR</i> 2 = 0.0455	<i>R</i> 1 = 0.0180, <i>wR</i> 2 = 0.0397	<i>R</i> 1 = 0.0147, <i>wR</i> 2 = 0.0335
goodness-of-fit on <i>F</i> <sup>2b</sup>	1.030	1.056	1.032
largest diff peak and hole (e Å <sup>-3</sup> )	1.427 and -0.827	1.764 and -0.767	1.476 and -0.495
	8	9	13
Crystal Data			
empirical formula	C <sub>18</sub> H <sub>31</sub> MoNO	C <sub>23</sub> H <sub>36</sub> MoN <sub>2</sub> O	C <sub>14</sub> H <sub>21</sub> MoNO
cryst habit, color	needle, yellow	needle, orange	square, orange
cryst size (mm)	0.25 × 0.10 × 0.10	0.25 × 0.03 × 0.03	0.55 × 0.50 × 0.30
cryst syst	monoclinic	orthorhombic	monoclinic
space group	<i>P</i> 2 <sub>1</sub> / <i>c</i>	<i>P</i> bca	<i>P</i> 2 <sub>1</sub> / <i>c</i>
volume (Å <sup>3</sup> )	1816.6(3)	4568.6(17)	1381.3(4)
<i>a</i> (Å)	10.6073(12)	17.536(4)	8.0187(12)
<i>b</i> (Å)	11.4737(11)	14.112(3)	13.3671(19)
<i>c</i> (Å)	15.0284(17)	18.461(4)	13.257(2)
α (deg)	90	90	90
β (deg)	96.675(6)	90	103.580(6)
γ (deg)	90	90	90
<i>Z</i>	4	8	4
density (calcd) (Mg/m <sup>3</sup> )	1.365	1.316	1.516
absorp coeff (mm <sup>-1</sup> )	0.722	0.588	0.934
<i>F</i> <sub>000</sub>	784	1904	648
Data Collection and Refinement			
measd reflns: total	37 598	21 820	18 348
measd reflns: unique	4193	5254	3177
final <i>R</i> indices <sup>a</sup>	<i>R</i> 1 = 0.0278, <i>wR</i> 2 = 0.0641	<i>R</i> 1 = 0.0410, <i>wR</i> 2 = 0.0778	<i>R</i> 1 = 0.0186, <i>wR</i> 2 = 0.0487
goodness-of-fit on <i>F</i> <sup>2b</sup>	1.112	0.985	1.079
largest diff peak and hole (e Å <sup>-3</sup> )	0.497 and -0.545	0.785 and -0.559	0.453 and -0.406
<sup>a</sup> <i>R</i> 1 on <i>F</i> = $\sum( F_o  -  F_c ) / \sum F_o $ ; <i>wR</i> 2 = $[\sum(F_o^2 - F_c^2)^2 / \sum w(F_o^2)^2]^{1/2}$ ; <i>w</i> = $[\sigma^2 F_o^2]^{-1}$ . <sup>b</sup> GOF = $[\sum(w( F_o  -  F_c )^2) / \text{degrees of freedom}]^{1/2}$ .			

Data for **5** were collected to a maximum 2θ value of 60.1° in 0.5° oscillations. The structure was solved by direct methods<sup>24</sup> and expanded using Fourier techniques. All non-hydrogen atoms were refined anisotropically, and all hydrogen atoms were included in fixed positions. The final cycle of full-matrix least-squares analysis was based on 6505 observed reflections and 242 variable parameters.

Data for **6** were collected to a maximum 2θ value of 60.1° in 0.5° oscillations. The structure was solved by direct methods<sup>24</sup> and expanded using Fourier techniques. All non-hydrogen atoms were refined anisotropically, and all hydrogen atoms were included in fixed positions. The final cycle of full-matrix least-squares analysis was based on 3854 observed reflections and 205 variable parameters.

Data for **8** were collected to a maximum 2θ value of 55.1° in 0.5° oscillations. The structure was solved by direct methods<sup>24</sup>

and expanded using Fourier techniques. All non-hydrogen atoms were refined anisotropically, and all hydrogen atoms were included in fixed positions. The final cycle of full-matrix least-squares analysis was based on 4193 observed reflections and 198 variable parameters.

Data for **9** were collected to a maximum 2θ value of 55.2° in 0.5° oscillations. The structure was solved by direct methods<sup>24</sup> and expanded using Fourier techniques. All non-hydrogen atoms were refined anisotropically, and all hydrogen atoms were included in fixed positions. The final cycle of full-matrix least-squares analysis was based on 5254 observed reflections and 252 variable parameters.

Data for **13** were collected to a maximum 2θ value of 55.1° in 0.5° oscillations. The structure was solved by direct methods<sup>24</sup> and expanded using Fourier techniques. All non-hydrogen atoms were refined anisotropically, and all hydrogen atoms were included in fixed positions. The final cycle of full-matrix

least-squares analysis was based on 3177 observed reflections and 159 variable parameters.

For each structure neutral-atom scattering factors were taken from Cromer and Waber.<sup>25</sup> Anomalous dispersion effects were included in  $F_{\text{calc}}$ ;<sup>26</sup> the values for  $\Delta f'$  and  $\Delta f''$  were those of Creagh and McAuley.<sup>27</sup> The values for mass attenuation coefficients are those of Creagh and Hubbell.<sup>28</sup> All calculations were performed using SHELXL-97<sup>29</sup> via the WinGX interface.<sup>30</sup> X-ray crystallographic data for all six structures are presented

(25) Cromer, D. T.; Waber, J. T. *International Tables for X-ray Crystallography*; The Kynoch Press: Birmingham, 1974; Vol. IV, Table 2.2 A.

(26) Ibers, J. A.; Hamilton, W. C. *Acta Crystallogr.* **1964**, 17, 781.

(27) Creagh, D. C.; McAuley, W. J. *International Tables for X-ray Crystallography*; Kluwer Academic Publishers: Boston, 1992; Vol. C, Table 4.2.6.8.

(28) Creagh, D. C.; Hubbell, J. H. *International Tables for X-ray Crystallography*; Kluwer Academic Publishers: Boston, 1992; Vol. C, Table 4.2.4.3.

(29) SHELXL-97; Sheldrick, G. M. *Acta Crystallogr.* **2008**, A64, 112.

(30) WinGX, V1.70; Farrugia, L. J. *J. Appl. Crystallogr.* **1999**, 32, 837.

(31) Frisch, M. J.; et al. *Gaussian 03*, Revision B.05; Gaussian, Inc.: Pittsburgh, PA, 2003.

(32) Parr, R. G.; Yang, W. *Density-Functional Theory of Atoms and Molecules*; Oxford University Press: Oxford, U.K., 1989.

(33) Becke, A. D. *J. Chem. Phys.* **1993**, 98, 5648.

(34) Lee, C.; Yang, W.; Parr, R. G. *Phys. Rev.* **1988**, B37, 785.

(35) Dunning, T. H., Jr.; Hay, P. J. In *Modern Theoretical Chemistry*; Schaefer, H. F., III, Ed.; Plenum Press: New York, 1976; pp 1–28.

(36) (a) Hay, P. J.; Wadt, W. R. *J. Chem. Phys.* **1985**, 82, 270. (b) Wadt, W. R.; Hay, P. J. *J. Chem. Phys.* **1985**, 82, 284. (c) Hay, P. J.; Wadt, W. R. *J. Chem. Phys.* **1985**, 82, 299.

in Table 3, and full details of all crystallographic analyses are provided in the Supporting Information.

**Computational Methods.** All theoretical calculations were performed using Gaussian03W<sup>31</sup> utilizing a DFT<sup>32</sup> method using the three-parameter exchange functional of Becke<sup>33</sup> and the correlation functional of Lee, Yang, and Parr (B3LYP).<sup>34</sup> Geometry optimizations were carried out using the LANL2DZ basis set, which included both Dunning and Hay's D95 sets for H, C, N, and O<sup>35</sup> and the relativistic electron core potential (ECP) sets of Hay and Wadt for W.<sup>36</sup> Frequency calculations on optimized geometries established that transition states possessed one and only one imaginary frequency whose atomic displacement vectors were consistent with the expected reaction pathway and that intermediates possessed either no imaginary frequencies or frequencies of negligible energy ( $< 50i \text{ cm}^{-1}$ ). Thermodynamic enthalpies and free energies are reported in kJ/mol as calculated at standard states (298.15 K and 1 atm).

**Acknowledgment.** We are grateful to The Dow Chemical Company for continuing support of this work, and we thank Drs. David Graf and Bill Tenn for assistance and helpful discussions. We also acknowledge Dr. Brian Patrick, Mr. Scott Semproni, and Mr. Rhett Baillie for technical assistance and the reviewers for constructive comments.

**Supporting Information Available:** Optimized structure and final thermochemical parameters of the various CpW(NO)(R)-( $\eta^3$ -allyl) complexes subjected to DFT calculations (PDF) and full details of the crystallographic analyses of complexes **3**, **5**, **6**, **8**, **9**, and **13** (CIF). This material is available free of charge via the Internet at <http://pubs.acs.org>.